

PEOPLE'S DEMOCRATIC REPUBLIC OF ALGERIA

MINISTRY OF HIGHER EDUCATION AND SCIENTIFIC RESEARCH



*UNIVERSITY OF SAAD DAHLEB*

*BLIDA 01- FACULTY OF TECHNOLOGY*

*MECHANICS DEPARTMENT*

**INDUSTRIAL TECHNOLOGY STUDY AND RESEARCH  
LABORATORY**

**L.E.R.T.I**

FINAL COURSE PROJECT FOR **MECHANICAL ENGINEERING  
DIPLOMAT** OBTENTION

Option **MATERIALS ENGINEERING.**

*THEME*

*synthesis and Characterization of New Ordered MAX Phases  
(**Cr<sub>2</sub>Ti Al C<sub>2</sub>**) By molten salt method.*

**Proposed and mentored by:**

**Dr. Youcef Hadji**

**carried out by:**

**Doudou Mohamed Islem - GM**

**Co-supervisor:**

**Dr. Bilal Cheniti (C.R.T.I Cheraga)**

**College Year 2023/2024**

## **Acknowledgments:**

*I first present my thanks to my supervisor Dr. Youcef Hadji for taking me as a candidate for this semester, guiding me throughout my journey from the very beginning, for showing empathy and tolerance towards my mistakes and situations.*

*Second, I want to thank all the members of L.E.R.T.I laboratory, for each individual has guided me through my experiment procedures with care, especially Mr. Saber Benamour & Mr. Hamzaoui Billal.*

*Without leaving off my dear U.M.M.K, descendants of good families group that I wish for each member to live a long long life.*

*Last but not least, I would like to direct my biggest thanks to my family members for supporting me throughout the toughest year of my life in many ways.*

### **Abstract:**

using the molten salt method, this study is about synthesising Ordered MAX phases by the elements (Cr, Ti, Al, and C), protected by KCl molten potassium chloride from oxidation under three temperatures (1000°C, 1100°C, and 1300°C) to reach the aimed phase.

### **Keywords:**

MAX phases, XRD, X ray diffraction, Ordered MAX phases, Cr<sub>2</sub>TiAlC<sub>2</sub>, molten salt method, sintering,

### **ملخص:**

هذه الدراسة تتناول تصنيع طور (MAX)

المرتب باستخدام عناصر (الكروم والتيتانيوم والألومنيوم والكربون) عن طريق طريقة الملح المنصهر، حيث يتم حماية المواد من الأكسدة باستخدام كلوريد (1000°C و 1100°C و 1300°C) البوتاسيوم المنصهر تحت ثلاث درجات حرارة

للوصول إلى الطور المستهدف

### **الكلمات المفتاحية:**

MAX ، Cr<sub>2</sub>TiAlC<sub>2</sub> ، MAX ، حيود الأشعة السينية، XRD ، طور MAX ،

طريقة الملح المنصهر،

**Résumé :**

Cette étude porte sur la synthèse de phases MAX ordonnées en utilisant la méthode du sel fondu. Les éléments utilisés sont le chrome, le titane, l'aluminium et le carbone, protégés de l'oxydation par le chlorure de potassium fondu à trois températures différentes (1000°C, 1100°C et 1300°C) afin d'atteindre la phase visée.

**Mots clés :**

les phases MAX Ordonnée, diffraction des rayons X, DRX,  $\text{Cr}_2\text{TiAlC}_2$ , la méthode des sel fondu.

## Contents :

### **CHAPTER I : Bibliographic research on MAX phases.**

I.1. MAX Phases history	11
I.2. Crystal structure	14
I.3 Electronic structure of MAX phases	17
I.4 Microstructure of MAX phases	18
I.5 Elaboration techniques used for MAX phases	19
I.5.1 Combustion synthesis	19
I.5.2 Hot pressing	20
<b>I.5.3 spark plasma sintering :</b>	<b>21</b>
I.5.4 The molten salt synthesis MS3	22
I.6. MAX phases properties	24
I.6.1 Elastic properties	24
I.6.3 Mechanical properties	27
I.6.3.1 High-Temperature Mechanical Behavior	28
I.6.3.2 Room Temperature Mechanical Behavior	29
I.6.4 Electronic properties	29
I.6.5 Thermal characteristics	30
I.7. State of the art	32
I.8. Conclusion	34

### **CHAPTER II: Experimentation techniques**

<b>Introduction:</b>	<b>36</b>
<b>Methodology:</b>	<b>36</b>
II.1.1 The Cr <sub>2</sub> Ti AlC <sub>2</sub> MAX phase synthesis	36
II.1.2 Weighing the powder	38
II.1.3 Grinding	40
II.1.4 cold compaction	41
II.1.5 Self encapsulation	43
II.1.6 Heat treatment by sintering	44

II.1.6.1 sample pot preparation	44
II.1.6.2 the furnace process	46
II.1.7 powders recovery	48
II.2. Microstructural Characterization:	51
II.2.1 X Ray Diffraction and Bragg's law	51
II.2.1.1. Interaction with Electron Clouds	51
II.2.1.2. Constructive and Destructive Interference	52
II.2.1.3 Experimental Observations	52
II.2.1.4 Structural Analysis	
<b>Chapter III: Results presentation &amp; Interpretation</b>	
III.1 Introduction:	55
III.2. X ray diffraction analysis of the powders $\text{Cr}_2\text{Ti AlC}_2$ & $\text{Cr}_2\text{Ti Al}_{1.2}\text{C}_2$ with Potassium Chloride KCl at $1000^\circ\text{C}$ - $1100^\circ\text{C}$ - $1300^\circ\text{C}$ .	56
III.3 Comparison of the three X Ray Diffraction graphs:	57
III.4. Final analysis and conclusion:	59
References: in the APA citation 7 <sup>th</sup> edition.	60
<b>Figure III.1:</b> XRD graph for the sample $\text{Cr}_2\text{Ti AlC}_2$ at $1000^\circ\text{C}$ coated with potassium chloride.	56
<b>Figure III.2:</b> XRD graph for the sample $\text{Cr}_2\text{Ti AlC}_2$ at $1100^\circ\text{C}$ coated with potassium chloride.	56
<b>Figure III.3:</b> XRD graph for the sample $\text{Cr}_2\text{Ti AlC}_2$ at $1300^\circ\text{C}$ coated with potassium chloride.	57
<b>Figure III.4:</b> XRD for the three samples stacked for comparison.	58

## **Figures list:**

**Figure I 1.1** Elements of the Periodic Table found in MAX phases and unit cell for  $n = 1$

**Figure I 1.2:** SEM pictures of the characteristic layered structure and mechanical response of some examples of MAX phases  $Ti_2AlC$ ,  $Cr_2AlC$ ,  $Ti_3SiC_2$ , and  $Ti_3AlC_2$

**Figure I 2.1:** . Crystal structure of the 211, 312, and 413 MAX phases. From Barsoum

**Figure I.2.2 :** (a) Schematic representation of the plane (110) of an  $M_3AX_2$  phase, (b) Replacement of planes A by planes C which results in a twinned structure, (c) twinning by rotation around the axis shown in (b) leads to the (110) plane of  $TiC$ .

**Figure I.4.1:** The three types of structures obtained: diagram of the structure and optical microscope observations of the surfaces in the directions parallel and perpendicular to the surface respectively.

**Figure I.5.1 :** Scheme of the basic steps during the combustion synthesis process.

**Figure I.5.2:** (a) Schematic diagram of hot pressing high-frequency induction heated sintering apparatus, (b) Photo of the heated die.

**Figure I.5.3. :** Working schematic of a SPS apparatus.

**Figure I.5.4 :** (a) MS3 step by step procedure.

**Figure I.6.1 :** Comparison of experimental and theoretical (a) bulk moduli  $B$  (red ) and (b) Young's moduli  $E$  (blue) of select MAX phases.

**Figure I.6.3.1 :** (a) Engineering stress-strain curves of 2-mm cubes of highly oriented samples of  $Ti_3SiC_2$ . The inset (right) shows a schematic of the cube and basal plane orientations. (b) Optical microscope micrograph of a polished and etched sample after deformation parallel to the basal planes. Note kinking at the corners. The kink band in the lower left corner generates a shear band that cuts across the cube face.

**Figure I.6 :** Characteristics of the MAX phase ceramics

**Figure I.6 :** Characteristics of the MAX phase ceramics

**Figure II.3:** precision analytical balance ADAM

**Figure II.4:** homogenized powder through baring balls.

**Figure II.5 :** powder compaction tool.

**Figure II.6 :** Manual Press 25 ton Hydraulic Pellet Press - Specac Ltd

**Figure II.7 :** sample tablet after compaction in the manual press

**Figure II.8 :** encapsulation/compaction tool and the pressure applied.

**Figure II.9 :** samples before and after encapsulation

**Figure II.10:** sintering pot filling steps.

**Figure II.11:** Tubular furnace Nabertherm GmbH 1800°C

**Figure II.12:** sample inside the Tubular furnace Nabertherm GmbH 1800°C at C.R.T.I cheraga research center.

**Figure II.13:** furnace Nabertherm B180

**Figure II.14:** sample pot state after recovery from the furnace.

**Figure II.15:** magnetic stirrer/heater Heifolph.

**Figure II.16:** the filtering/rinsing process tools (Conical flask/Erlenmeyer, filter, plastic funnel)

**Figure II.17:** Memmert Single Display UN Series Universal Oven.

**Figure II.18 :** Diffractometer Bruker D2 PHASER.

**Figure III.1:** XRD graph for the sample Cr<sub>2</sub>Ti Al C<sub>2</sub> at 1300°C.

**Figure III.2:** XRD graph for the sample Cr<sub>2</sub>Ti AlC<sub>2</sub> at 1300°C.

**Figure III.3:** XRD graph for the sample Cr<sub>2</sub>Ti Al<sub>1.2</sub> C<sub>2</sub> at 1300°C.

**Figure III.4:** XRD for the three samples stacked for comparison.



## Tables list :

**Table 1:** The known  $M_{n+1}AX_n$  phases, sorted by stoichiometry (“211”, “312”, and “413”) and valence electron configuration for the M and A elements.


**Table 2 :** Density, shear modulus G, Young’s modulus E, and Poisson’s ratio  $\nu$  of select MAX phases. Also listed are the bulkmoduli values measured directly in an anvil cell ( $B^*$ ) and bulkmoduli values calculated from the shear and longitudinal soundvelocities ( $B_{\ddagger}$ )

**Table 3 :** The theoretical calculations of the state's position of  $Zr_2InC$  (C-p and C-s)

**Table 4 :** Shows the determined transverse, longitudinal, average sound velocity ( $v_t, v_l$ , and  $v_m$  in m/s) and density ( $r$  in  $g/cm^3$ ), the minimum thermal conductivity  $K_{min}$  ( $W\ m^{-1}\ K^{-1}$ ) and the debye temperatures ( $\theta_D$  in K) for the  $Zr_2AC$  MAX phase.

**Table 5:** tribological conditions used for the composite systems.

**Table 6 :** Elaborated samples mass in gram.



***Chapter I:  
bibliographic research  
on MAX phases***

## I.1. MAX Phases history:

In the 1960s, Hans Nowotny's research team in Vienna achieved an extraordinary feat by discovering more than 100 new carbides and nitrides, including the so-called "H phases" and their derivatives  $Ti_3SiC_2$  and  $Ti_3GeC_2$ . Despite this remarkable discovery, these phases remained largely uninvestigated until the 1990s when researchers began to take a renewed interest.

The revitalization of research on these phases began in the mid-1990s when Barsoum and El-Raghy successfully synthesized relatively pure samples of  $Ti_3SiC_2$  and discovered a material with a unique combination of metallic and ceramic properties. This material exhibited high electrical and thermal conductivity, similar to metals, and was machinable. However, it also had exceptional resistance to oxidation and thermal shock, like ceramics.

Later, when Barsoum and El-Raghy discovered  $Ti_4AlN_3$ , it became clear that these phases shared a basic structure that gave them similar properties. This realization led to the introduction of the nomenclature " $M_{n+1}AX_n$  phases" ( $n=1, 2, \text{ or } 3$ ) or "MAX phases", where M is a transition metal, A is an A-group element, and X is C and/or N.

Until around twelve years ago, the MAX phases represented an unexplored class of materials that have since revealed exceptional chemical, physical, electrical, and mechanical characteristics.

These phases have been found to exhibit a range of extraordinary properties, such as reversible dislocation-based deformation, high specific stiffness with excellent machinability, and outstanding thermal and electrical conductivity, among others.

Their deformation mechanism involves a combination of kink and shear band formation, along with delaminations within grains. Some MAX phases also demonstrate remarkably low friction coefficients. These remarkable properties arise from the layered structure of the MAX phases and the unique mixed metallic-covalent nature of the M–X bonds, which are exceptionally strong, coupled with relatively weak M–A bonds.

The distinctive blend of properties in MAX phases highlights their potential for applications in high-temperature structures, protective coatings, sensors, low-friction surfaces, electrical contacts,

tunable damping films for microelectromechanical systems, and various other areas. The ability to harness the exceptional metallic and ceramic properties of MAX phases has spurred a rapid increase in global research efforts and commercialization in this field.[3]

A element	S <sup>2</sup> (group 12)	S <sup>2</sup> p <sup>1</sup> (group 13)	S <sup>2</sup> p <sup>2</sup> (group 14)	S <sup>2</sup> p <sup>3</sup> (group 15)	S <sup>2</sup> p <sup>4</sup> (group 16)
<b>211 phases</b>					
<b>M 3d</b>	<b>Ti<sub>2</sub>CdC</b>	<b>Sc<sub>2</sub>InC</b>			<b>Ti<sub>2</sub>SC<sub>2</sub></b>
		<b>*Ti<sub>2</sub>AlC</b>	<b>*Ti<sub>2</sub>GeC</b>		
		<b>Ti<sub>2</sub>GaC</b>	<b>*Ti<sub>2</sub>SnC</b>		
		<b>Ti<sub>2</sub>InC</b>	<b>Ti<sub>2</sub>PbC</b>		
		<b>Ti<sub>2</sub>TiC</b>			
		<b>*VAlC</b>	<b>*V<sub>2</sub>GeC</b>	<b>V<sub>2</sub>PC</b>	
		<b>V<sub>2</sub>GaC<sub>2</sub></b>		<b>VAsC</b>	
		<b>*Cr<sub>2</sub>AlC</b>	<b>Cr<sub>2</sub>GeC</b>		
		<b>Cr<sub>2</sub>GaC</b>			
		<b>*Ti<sub>2</sub>AlN<sub>2</sub></b>			
		<b>Ti<sub>2</sub>GaN</b>			
		<b>TiInN</b>			
		<b>V<sub>2</sub>GaN</b>			
		<b>Cr<sub>2</sub>GaN<sub>2</sub></b>			
<b>M 4d</b>		<b>Zr<sub>2</sub>InC</b>	<b>Zr<sub>2</sub>SnC</b>		<b>Zr<sub>2</sub>SC</b>
		<b>Zr<sub>2</sub>TiC</b>	<b>Zr<sub>2</sub>PbC<sub>2</sub></b>		
		<b>*NbAlC</b>	<b>Nb<sub>2</sub>SnC</b>	<b>Nb<sub>2</sub>PC</b>	<b>Nb<sub>2</sub>SC</b>
		<b>Nb<sub>2</sub>GaC</b>		<b>Nb<sub>2</sub>AsC</b>	
		<b>NbInC</b>			
		<b>Mo<sub>2</sub>GaC<sub>2</sub></b>			
		<b>Zr<sub>2</sub>InN</b>			
		<b>Zr<sub>2</sub>TiN</b>			
<b>M 5d</b>		<b>Hf<sub>2</sub>InC</b>	<b>Hf<sub>2</sub>SnC</b>		<b>Hf<sub>2</sub>SC</b>
		<b>Hf<sub>2</sub>TiC</b>	<b>Hf<sub>2</sub>2PbC</b>		
		<b>Ta<sub>2</sub>AlC<sub>2</sub></b>	<b>Hf<sub>2</sub>SnN</b>		
		<b>Ta<sub>2</sub>GaC</b>			

<b>312 phases</b>	
<b>M 3d</b>	*Ti <sub>3</sub> AlC <sub>2</sub> *Ti <sub>3</sub> SiC <sub>2</sub>
	*V <sub>3</sub> AlC <sub>2</sub> (or (V,Cr) <sub>3</sub> Al <sub>2</sub> C <sub>2</sub> ) *Ti <sub>3</sub> GeC <sub>2</sub>
<b>M 5d</b>	Ta <sub>3</sub> AlC <sub>2</sub>
<b>413 phases</b>	
<b>M 3d</b>	Ti <sub>4</sub> AlN <sub>3</sub>
	V <sub>4</sub> AlC <sub>3</sub> TTi <sub>4</sub> SiC <sub>3</sub>
<b>M 4d</b>	Ti <sub>4</sub> GaC <sub>3</sub> ti <sub>4</sub> GeC <sub>3</sub>
<b>M 4d</b>	Nb <sub>4</sub> AlC <sub>3</sub>
<b>M 5d</b>	Ta <sub>4</sub> AlC <sub>3</sub>

**Table 1:** The known M<sub>n+1</sub>AX<sub>n</sub> phases, sorted by stoichiometry (“211”, “312”, and “413”) and valence electron configuration for the M and A elements.

H																	He
Li	Be											B	C	N	O	F	Ne
Na	Mg											Al	Si	P	S	Cl	Ar
K	Ca	Sc	Ti	V	Cr	Mn	Fe	Co	Ni	Cu	Zn	Ga	Ge	As	Se	Br	Kr
Rb	Sr	Y	Zr	Nb	Mo	Tc	Ru	Rh	Pd	Ag	Cd	In	Sn	Sb	Te	I	Xe
Cs	Ba	Lu	Hf	Ta	W	Re	Os	Ir	Pt	Au	Hg	Tl	Pb	Bi	Po	At	Rn

M

Transition metal

A

Group A element

X

C or N

**M<sub>n+1</sub>AX<sub>n</sub>**  
n = 1, 2 or 3

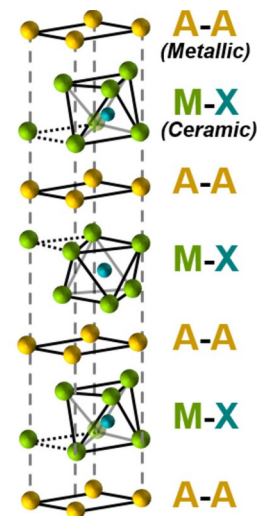


**Figure I 1.1** Elements of the Periodic Table found in MAX phases and unit cell for n = 1

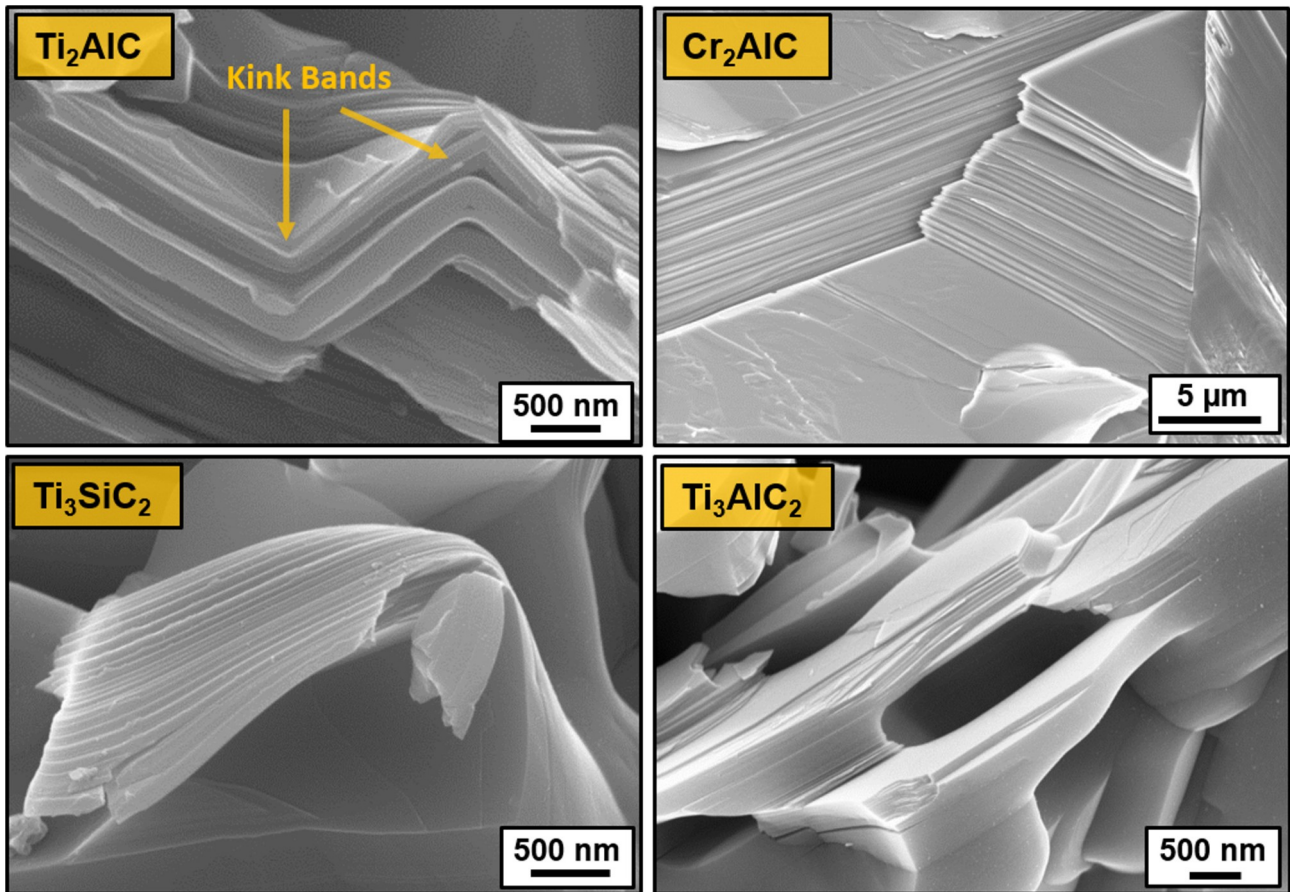


**Figure I 1.2:** SEM pictures of the characteristic layered structure and mechanical response of some examples of MAX phases  $Ti_2AlC$ ,  $Cr_2AlC$ ,  $Ti_3SiC_2$ , and  $Ti_3AlC_2$

### I.2. Crystal structure:

As defined by Barsoum [2], The MAX phases follow a general formula of  $M_{n+1}AX_n$ , where  $n=1, 2$ , or  $3$ . The different stoichiometries of MAX phases are often referred to as 211 ( $n=1$ ), 312 ( $n=2$ ), and 413 ( $n=3$ ). The M elements are transition metals from groups 3 (Sc), 4 (Ti, Zr, Hf), 5 (V, Nb, Ta), and 6 (Cr and Mo). No MAX phases with the group-3 elements Y or Lu, or the group-6 element W, have been discovered.

The A element is from groups 12 (Cd), 13 (Al, Ga, In, Tl), 14 (Si, Ge, Sn, Pb), 15 (P, As), or 16 (S) of the periodic table. The "A" label originates from the old American nomenclature for the periodic table. The X element is C and/or N, and the terms "MAC phases" and "MAN phases" are sometimes used to refer to the MAX phase carbides (X C) and nitrides (X N), respectively. Table 1 provides a comprehensive list of all MAX phases known to date.

Fig.I 2.1 displays the hexagonal unit cells of the 211, 312, and 413 MAX phases. These unit cells consist of M 6 X octahedra (e.g., Ti 6 C) interlayered with sheets of A elements, such as Si or Ge. The number of M layers separating the A layers varies among the structures: in the 211 phases, there are two M layers; in the 312 phases, three M layers; and in the 413 phases, four M layers. The M 6 X edge-sharing octahedral building block in the MAX phases is identical to that in the binary carbides and nitrides, MX.

In the 312 and 413 MAX structures, there are two distinct M sites: those adjacent to A (M(1)) and those not (M(2)). In the 413 structure, there are also two non-equivalent X sites, X(1) and X(2). The MX layers in the MAX phases are twinned with respect to each other and separated by the A layer, which acts as a mirror plane. This is demonstrated in Figure 2, a high-resolution transmission electron microscopy (TEM) image acquired along the  $[11\bar{2}0]$  zone axis of Ti<sub>3</sub>SiC<sub>2</sub>. The twinning and the characteristic "zig-zag" stacking of the MAX phases are evident in this image.

The MAX structures are anisotropic, with lattice parameters typically around  $a \sim 3 \text{ \AA}$  and  $c \sim 13 \text{ \AA}$  (for 211 phases),  $c \sim 18 \text{ \AA}$  (for 312 phases), and  $c \sim 23\text{-}24 \text{ \AA}$  (for 413 phases).

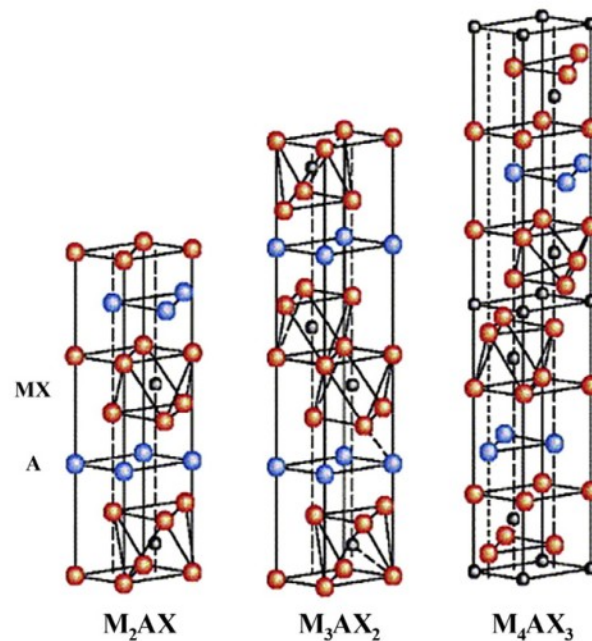


**Figure I 2.1:** . Crystal structure of the 211, 312, and 413 MAX phases. From Barsoum[2].

There are many similarities between the  $M_{n+1}AX_n$  phase and the stoichiometric binary compound  $M_{n+1}AX_n$  in terms of structure and properties, as demonstrated by Barsoum[2]. The transformation of  $Ti_3SiC_2$  into  $TiC$  by a three-step process is an example of this similarity, as shown schematically in Figure 1.6 for a  $M_3AX_2$  compound.

The first step involves replacing the A atoms with X atoms, resulting in a macle structure every three M planes where the planes previously occupied by the A atoms are now mirror planes (**Figure I.2.2 (a)**). The second step removes the macle between adjacent  $M_3X_2$  units by rotating around an axis perpendicular to the c-axis (**Figure I.2.2 (b)**). This results in a (110) plane of  $TiC$  (**Figure I.2.2 (c)**).

In the case of  $Ti_3SiC_2$ , this transformation is associated with a 15% reduction in the volume of the unit cell. This transformation is one of the preferred modes by which  $Ti_3SiC_2$  reacts and decomposes.

Overall, the similarities between the  $M_{n+1}AX_n$  phase and the stoichiometric binary compound  $MX$ , as well as the ability to transform one into the other, highlight the potential for MAX phases to be used in a wide range of applications where both high strength and electrical conductivity are required. The ability to tailor the properties of MAX phases through variations in the M, A, and X elements, as well as through the use of different synthesis methods, makes them a promising material for future research and development.



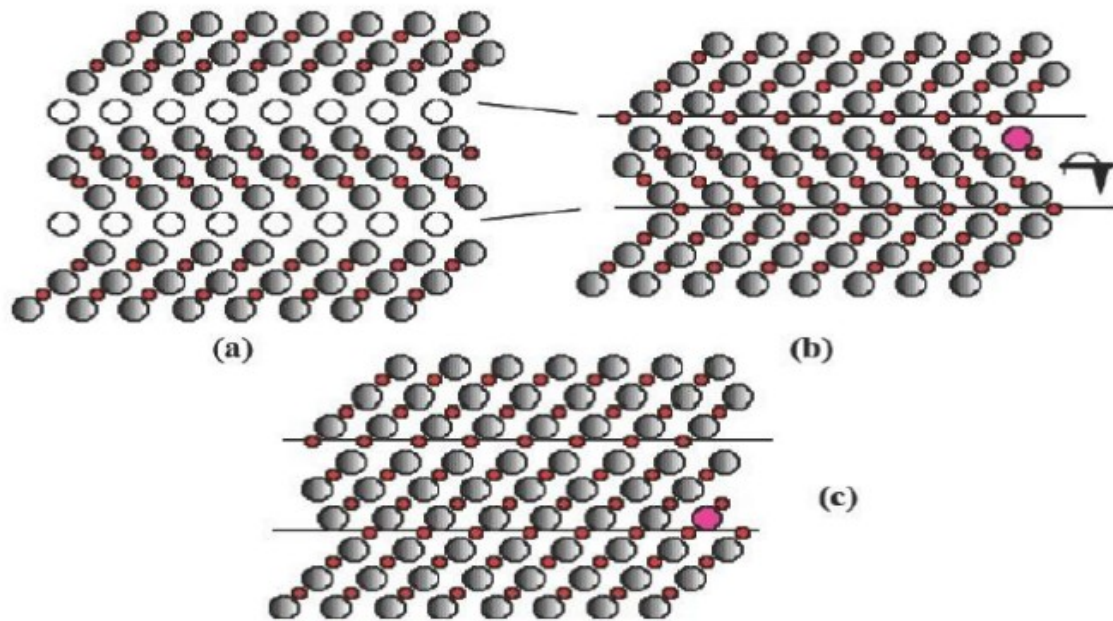


**Figure I.2.2 :** (a) Schematic representation of the plane (110) of an  $M_3AX_2$  phase, (b) Replacement of planes A by planes C which results in a twinned structure, (c) twinning by rotation around the axis shown in (b) leads to the (110) plane of TiC.

### I.3 Electronic structure of MAX phases :

In general, the primary interatomic bonds in MAX phases can be summarized as follows:

- a) the M and X atoms in MAX phases form a strong covalent bond in the M-X layers, which leads to a high degree of rigidity in these materials. This is because covalent bonds involve the sharing of electrons between atoms, leading to a strong attractive force between them.
- b) The M-A bond, on the other hand, is generally weaker than the M-X bond. This is because the A atoms in MAX phases are typically larger and less electronegative than the M and X atoms, leading to weaker interactions between them.
- c) the metallic bond M d -M d dominates the density of states at the Fermi level. This bond involves the overlap of the d orbitals of the M atoms, leading to a high density of states at the Fermi level. This is important because the density of states at the Fermi level is directly related to the electrical conductivity of a material. In particular, a high density of states at the Fermi level leads to good electrical conductivity, which is why MAX phases are typically good conductors of electricity. Overall, the combination of strong covalent bonds in the M-X layers and high electrical conductivity due to the metallic bond M d -M d makes MAX phases highly desirable for a wide range of applications, including aerospace, automotive, and energy storage.[4]

#### **I.4 Microstructure of MAX phases:**

The general structure of a ceramic can consist of grains of the same phase or different phases, separated by grain boundaries. Defects, related to the manufacturing processes, may also be present and weaken the structure. These defects can be either residual porosities after sintering or microcracks that appear at the grain boundaries during cooling.

In the research done by A. Souchet et al, The powder used in the process has the advantage of having a sufficiently fine particle size, where each grain is a single crystal and the grains are shaped like petals. The powder is then compacted by vibration in the cold pressing mold to orient these petals parallel to the surface on which pressure will be applied. Although this technique is rather crude, it still yields good results in terms of grain alignment, as shown by the images corresponding to structures B and C in the (figure **I.4.1**), (**images B.b et C.b**) highlights the different structures obtained from this process.[16]

The three types of MAX phases Microstructure that can be observed according to Nieświec, M et al [7] are:

1. Fine-grained microstructure (FG): MAX phases with a fine-grained microstructure have a high dislocation density and a high density of grain boundaries, which can lead to improved mechanical properties.
2. Coarse-grained microstructure (CG): MAX phases with a coarse-grained microstructure have larger grains and fewer grain boundaries, which can lead to improved thermal properties.
3. Mixed microstructure: MAX phases with a mixed microstructure have a combination of fine and coarse grains, with the fine grains distributed in a coarse-grained matrix. This microstructure can lead to improved mechanical and thermal properties.[7]

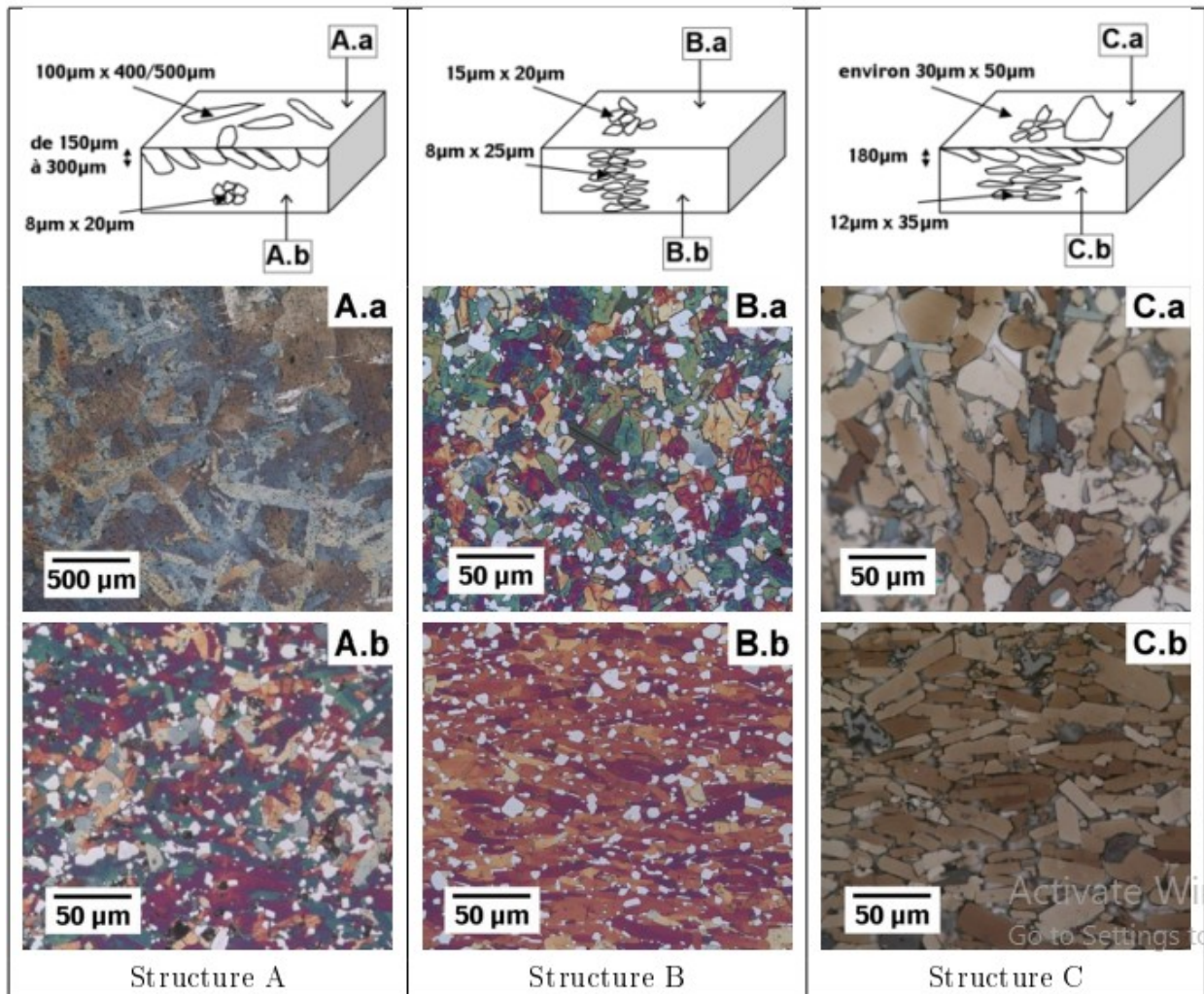


**Figure I.4.1:** The three types of structures obtained: diagram of the structure and optical microscope observations of the surfaces in the directions parallel and perpendicular to the surface respectively

## I.5 Elaboration techniques used for MAX phases:

**I.5.1 Combustion synthesis:** According to (Истомин et al., 2024), Combustion synthesis (CS) involves self-propagating high-temperature synthesis (SHS) and volume combustion synthesis (VCS) as two modes of synthesis. In SHS, a self-sustained reaction rapidly propagates through a mixture of reactants, while in VCS, the entire sample is uniformly heated until the reaction occurs simultaneously throughout the volume. CS offers advantages such as short synthesis times, energy savings, simple equipment, and the ability to produce high-purity products. The article emphasizes the increasing number and variety of products produced by CS, including carbides, borides, and silicides.[8]

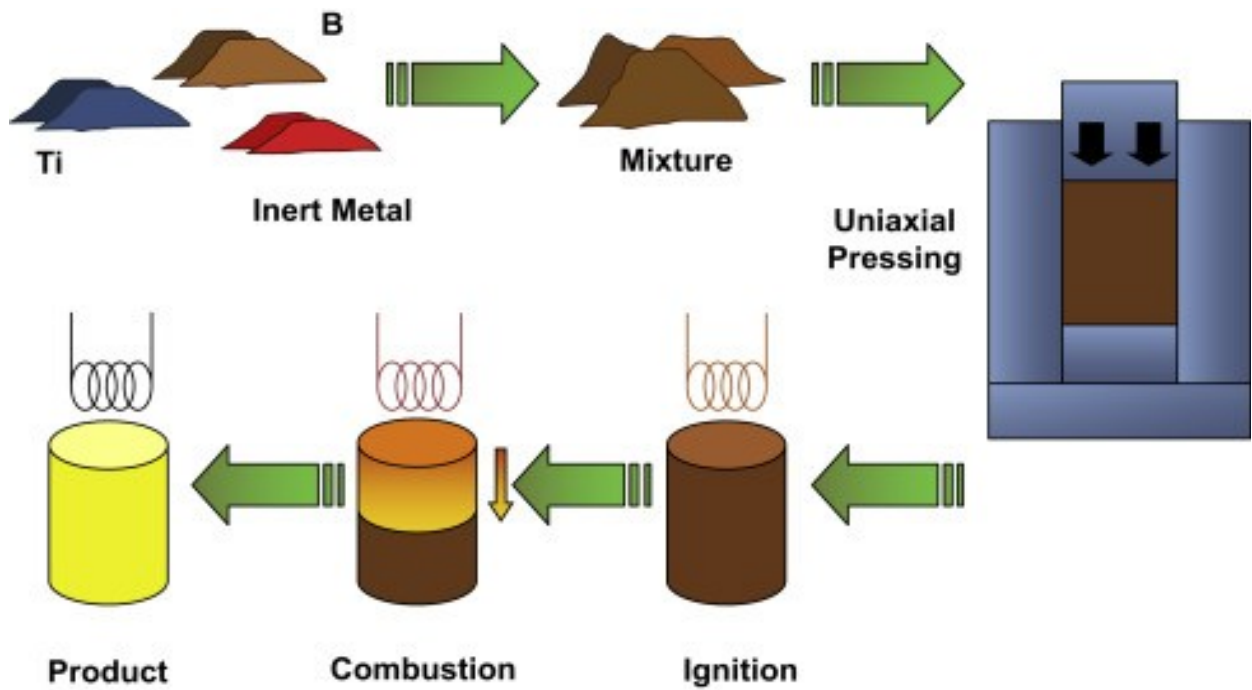


**Figure I.5.1** :Scheme of the basic steps during the combustion synthesis process.[9]

### **I.5.2 Hot pressing:**

Hot pressing is a crucial technique in materials processing, particularly in the fabrication of advanced materials like MAX phases. This method involves compacting powders at elevated temperatures, leading to densification and sintering of the material. Hot pressing is known for its ability to produce high-density products with improved mechanical and thermal properties. The process is often used in the manufacturing of carbide cutting tools and specialized applications due to its effectiveness in achieving high-quality, high-strength components. Additionally, hot pressing can be combined with sintering to create complex shapes and structures, making it a versatile and widely used method in the production of various materials.

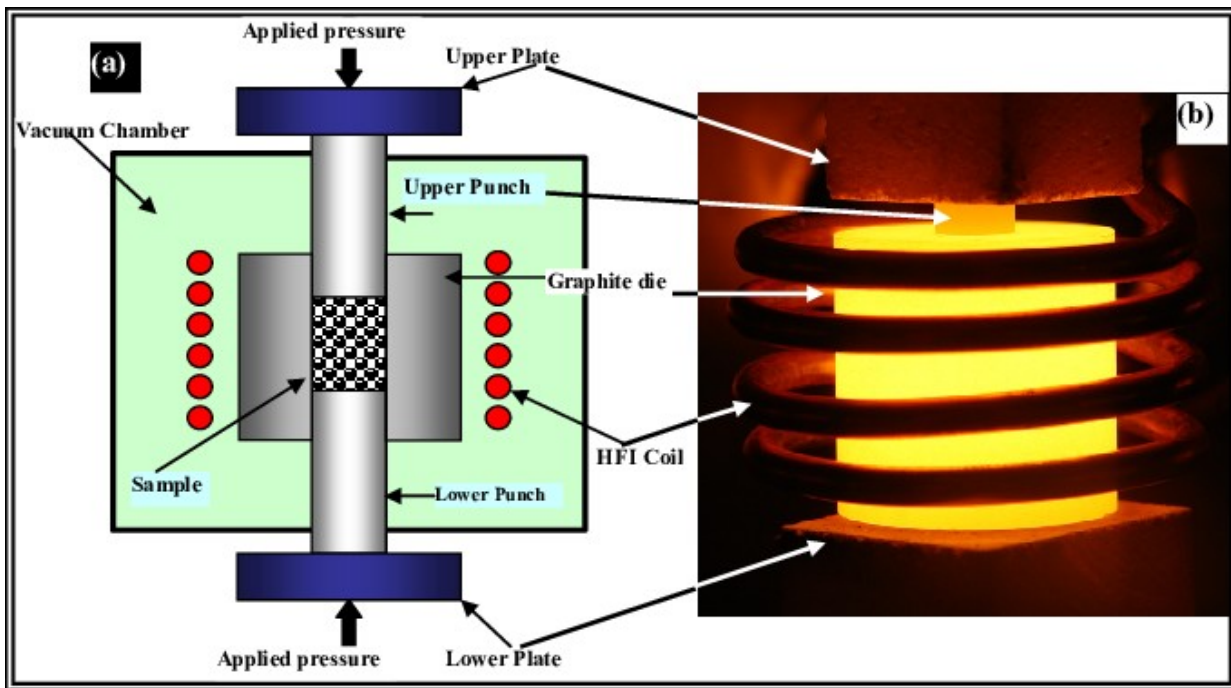


**Figure I.5.2:** (a) Schematic diagram of hot pressing high-frequency induction heated sintering apparatus, (b) Photo of the heated die.[10]

**I.5.3 spark plasma sintering :** FAST/SPS technology utilizes a mechanical loading system that doubles as a high-power electrical circuit within a controlled environment. The materials' good electrical conductivity allows for the generation of high currents with low voltages, leading to efficient Joule heating. This system enables the transfer of heat even to electrically non-conductive sintering powder. By adjusting pulse and pause durations, sintering cycles with rapid heating rates of up to  $1000\text{ }^{\circ}\text{C min}^{-1}$  are achievable, reducing process duration and energy costs significantly. The process involves applying uniaxial mechanical pressure to enhance densification, typically ranging between 50 and 250 kN. Control of the process is primarily through temperature measurement using various methods, with maximal temperatures reaching up to  $2400\text{ }^{\circ}\text{C}$  when using standard graphite tools. The choice of heating the sample or the die depends on the electrical resistance of the components and the sample material itself (Guillon et al., 2014).[11]

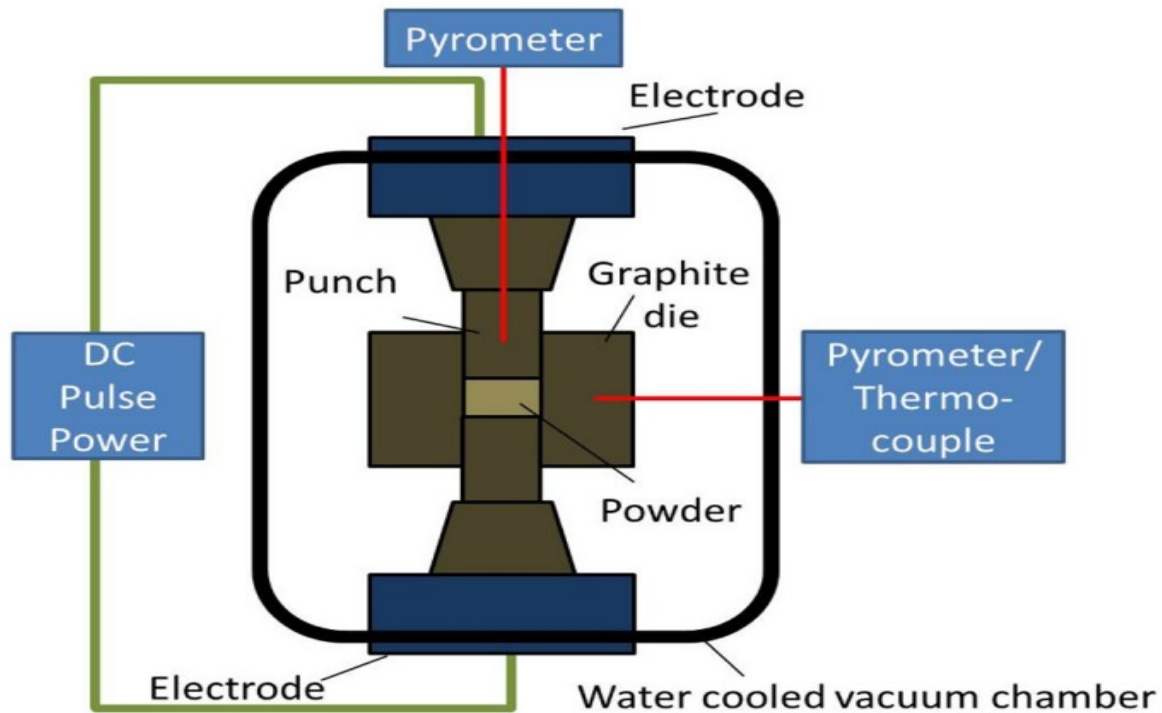


**Figure I.5.3. :** Working schematic of a SPS apparatus.

#### **I.5.4 The molten salt synthesis MS3 :**

Molten Salt-Shielded Synthesis (MS3) is an innovative method for the rapid and efficient synthesis of MAX phases and MXenes in the open air environment. This technique utilizes Lewis-acid salts as a shield to facilitate the synthesis process. The MS3 method involves the use of molten salts to shield the reaction from the surrounding air, enabling the synthesis of MAX phases and MXenes with high purity and yield. The process involves the preparation of a mixture of MAX phase precursor and eutectic salt, followed by pressing into a pellet and heating in a crucible with a salt mixture covering the surface. The molten salt shield separates the MAX phase from the air, allowing for controlled etching reactions to occur at elevated temperatures. After the etching process, the samples are washed and filtered to obtain the final MS3-MXene products. This method offers scalability and can be applied to large batches of MAX phases, making it a significant advancement in the synthesis of MAX phases and MXenes for both scientific research and industrial applications[12]. This procedure follows these steps :

- a) **Preparation of Precursor Materials:** The first step involves preparing the precursor materials, which typically include the MAX phase precursor and the eutectic salt. The precursor materials are crucial for initiating the synthesis process.

- b) **Mixing of Precursor Materials:** The next step is to mix the MAX phase precursor and the eutectic salt in the desired ratio. This mixture will serve as the starting material for the synthesis process.
- c) **Pellet Formation:** The mixed precursor materials are then pressed into a pellet or compacted into a specific shape. This step is essential for ensuring uniformity and compactness of the starting material.
- d) **Heating with Molten Salt Shield:** The pellet is then heated in a crucible with a salt mixture covering the surface. The molten salt shield plays a critical role in protecting the reaction from the surrounding air, enabling controlled etching reactions to occur at elevated temperatures.
- e) **Etching Process:** The molten salt shield allows for controlled etching reactions to take place, leading to the transformation of the MAX phase precursor into the desired MAX phase or MXene product. This step is crucial for the synthesis of high-purity materials.
- f) **Cooling:** After the etching process is complete, the samples are cooled to room temperature. This step is essential for solidifying the MAX phase or MXene products and ensuring their structural integrity.
- g) **Washing:** The cooled samples are then washed in water to remove any residual salts or impurities. This step is crucial for purifying the synthesized materials and ensuring their quality.
- h) **Filtering:** The washed samples are then filtered to remove any remaining impurities and obtain the purified synthesized materials. This step is essential for obtaining high-purity MAX phase or MXene products with controlled properties and characteristics.

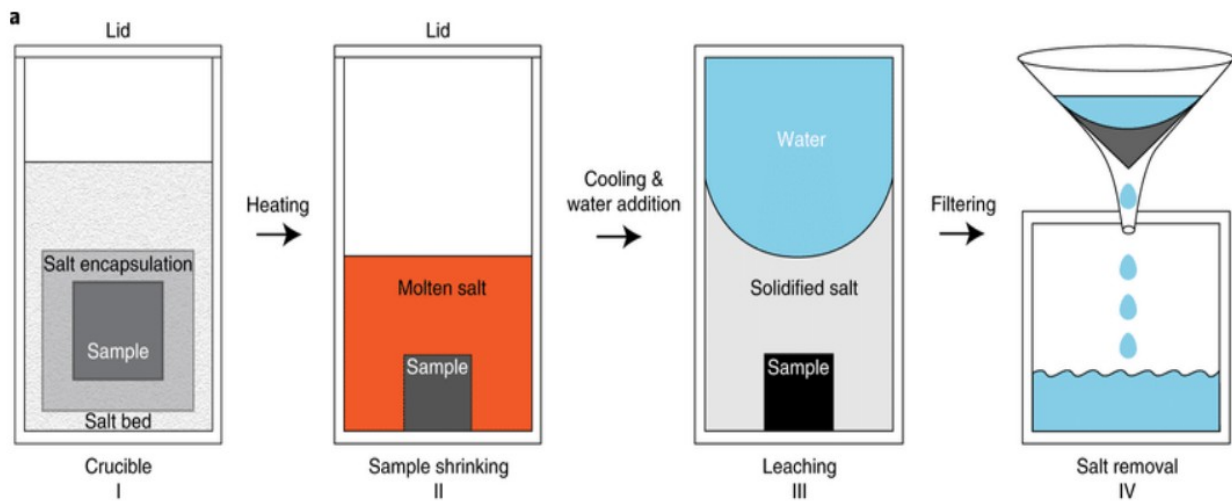


**Figure I.5.4 :** (a) MS3 step by step procedure.

- these are the most used elaboration methods used for MAX phases among others like :

- ◆ Chemical vapor deposition
- ◆ Physical vapor deposition
- ◆ Arc melting
- ◆ Reactive sintering
- ◆ Plasma spraying
- ◆ Laser cladding
- ◆ Mechanical alloying

These techniques can be used to synthesize MAX phases with a range of properties, including high strength, high toughness, and high electrical conductivity. The choice of technique depends on the desired properties of the MAX phase, as well as the availability of starting materials and the required processing conditions[12].

## **I.6. MAX phases properties :**

### **I.6.1 Elastic properties :**

MAX phases are elastically stiff with high specific stiffness and low Poisson's ratios. They are easily machinable, unlike other materials with high stiffness. The elastic properties of MAX phases vary based on composition, with In-, Pb-, and Sn-containing phases being less stiff. Theoretical calculations of elastic properties generally agree with experimental results, but there are exceptions. Stoichiometry and vacancy concentration affect the bulk modulus of MAX phases, and the basal planes can be corrugated, leading to changes in elastic properties. MAX phases are mildly anisotropic, and their elastic constants can be measured using acoustic techniques or diamond anvil



cells. The elastic properties of some MAX phases are not strongly affected by temperature. **Table 2** lists the elastic properties of the 312 MAX phases. The elastic constants  $c_{11}$ ,  $c_{12}$ ,  $c_{13}$ ,  $c_{33}$ , and  $c_{44}$  are presented for each MAX phase, with  $c_{66}$  calculated as  $(c_{11} - c_{12})/2$ . The table shows that the selected MAX phases are mechanically stable and meet the conditions for dynamic stability.[14]

Solid	Density (g cm <sup>-3</sup> )	G (GPa)	E (GPa)	$\nu$	B1 (GPa)	B* (GPa)
TiAlC	4.1	118	277	0.19	144	186
Ti <sub>2</sub> AlCo.sNo						
.s	4.2	123	290	0.18		
V <sub>2</sub> AlC	4.81	116	235	0.2	152	201
Cr <sub>2</sub> AlC <sub>2</sub>	5.24	102	245	0.2	138	166
	5.1	116	288			
Nb <sub>2</sub> AlC <sub>2</sub>	6.34	117	286	0.21	165	208
Ta <sub>2</sub> AlC	11.46	121	292			251
Ti <sub>3</sub> SiC <sub>2</sub>	4.52	139	343-339	0.2	190	206
Ti <sub>3</sub> GeC <sub>3</sub>	5.02	142	340-347	0.19	169	179
Ti <sub>3</sub> (Si,Ge)C <sub>3</sub>	4.35	136.8	322	0.18	166	183 + 4
Ti <sub>3</sub> AlC <sub>3</sub>	4.2	124	297	0.2	165	226 + 3
Ti <sub>3</sub> AlCN	4.5	137	330	0.21		219 + 4
Cr <sub>2</sub> GeC	6.88	80	245	0.29	165	182 + 2
						169 I 2
V <sub>2</sub> GeC						165 I 2
Ti <sub>2</sub> SC		125	290	0.16	145	191 I 3
Ti <sub>2</sub> SnC						152 + 3
Nb <sub>2</sub> SnC <sub>2</sub>			216			180 # 5
Zr <sub>2</sub> SnC			178			
Hf <sub>2</sub> SnC			237			169 + 4
Nb <sub>2</sub> AsC	8.05					224 + 2
Nb <sub>4</sub> AlC <sub>3</sub>	6.98	127	306			
B-TaAlC <sub>3</sub>	13.2	132	324			261 + 2
Ti <sub>4</sub> AlN <sub>3</sub>	4.7	127	310	0.22	185	216
TiC0.96	4.93	205	500	0.19	272	

**Table 2 :** Density, shear modulus G, Young's modulus E, and Poisson's ratio  $\nu$  of select MAX phases. Also listed are the bulkmoduli values measured directly in an anvil cell ( $B^*$ ) and bulk moduli values calculated from the shear and longitudinal soundvelocities ( $B^\ddagger$ )[14]

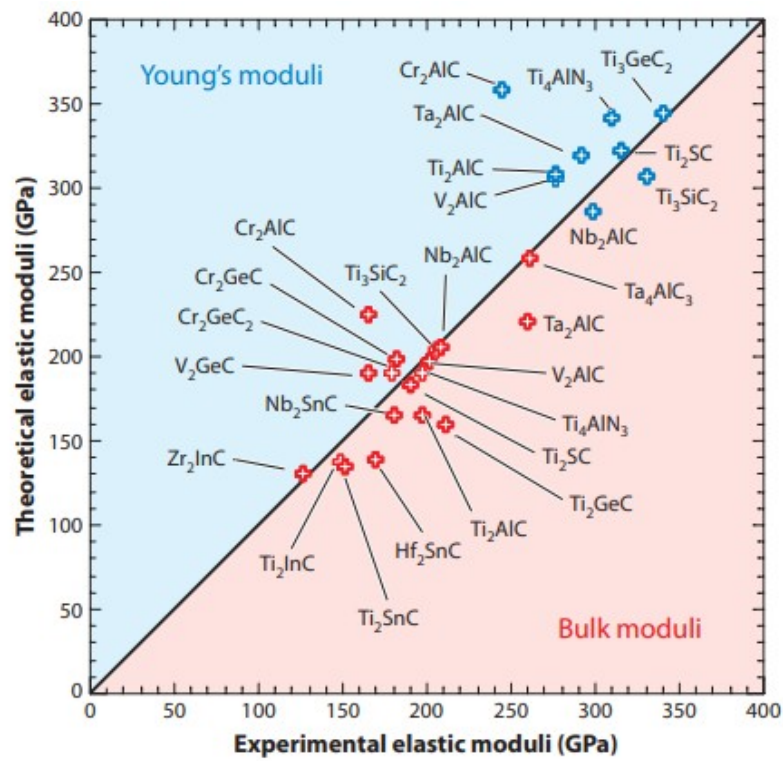
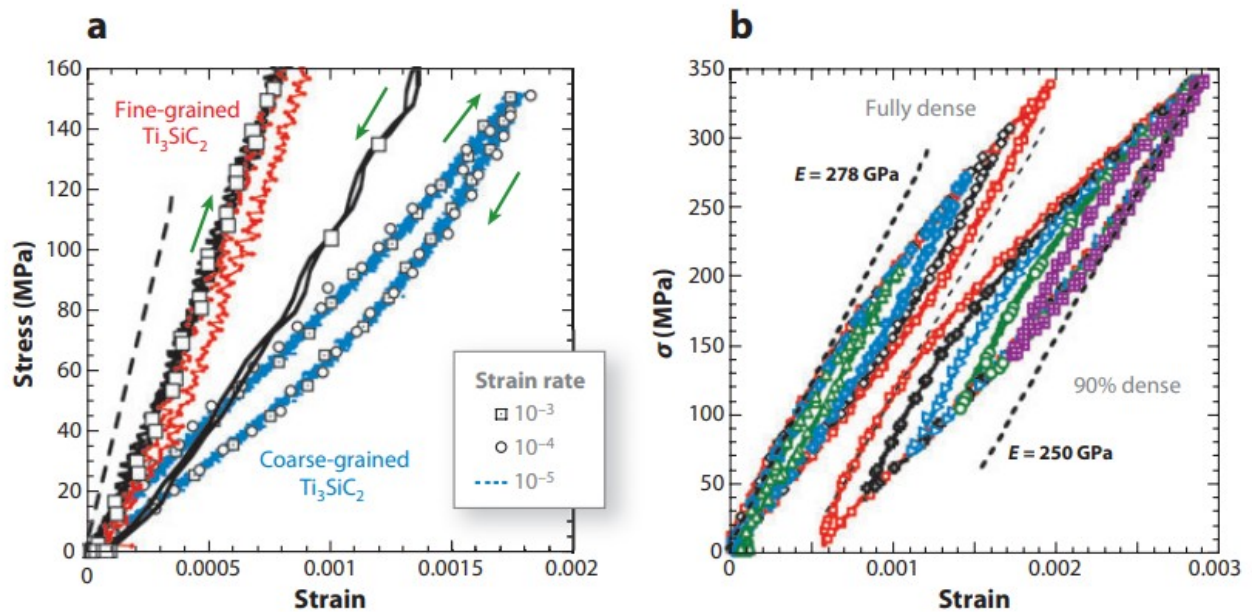


Figure I.6.1 : Comparison of experimental and theoretical (a) bulk moduli B (red ) and (b) Young's moduli E (blue) of selectMAX phases.



**Figure I.6.2.1** : Typical cyclic compressive reversible stress-strain loops. (a)  $Ti_3SiC_2$  samples showing the dramatic difference in response between coarse-grained (CG) samples (blue loops) and fine-grained (FG) samples (black and red loops). The small loops comprise three different loops obtained at three different strain rates that differ from each other by an order of magnitude each. Within the resolution of the measurement, the three loops are identical in shape and area. The red loop—obtained on the FG sample at 250 MPa—is significantly stiffer and is smaller in area than the CG loops. The green arrows denote the loading direction. (b)  $Ti_2AlC_2$  samples, with comparable grain sizes but slightly different densities. The set of nested loops for the 10-vol% porous sample are shifted to the right for clarity. The 10-vol% porous sample dissipated more energy, on an absolute basis, than its fully dense counterpart. Note the nested loops and only one loading trajectory on the left and one unloading trajectory on the right.

### I.6.3 Mechanical properties:

MAX phases are known for their high strength, stiffness, and damage tolerance, making them attractive for use in high-temperature applications. They exhibit a unique mode of deformation, known as kinking, which allows them to undergo large plastic strains without undergoing brittle fracture. This behavior is attributed to the layered structure of MAX phases, which allows for easy slip and twinning. The mechanical properties of MAX phases can be tailored by changing the composition and structure of the material. For example, increasing the  $n$  value in the formula leads to a decrease in strength and stiffness, while adding reinforcements such as carbon nanotubes or graphene can improve the mechanical properties.[14]

### I.6.3.1 High-Temperature Mechanical Behavior :

All MAX phases tested exhibit a brittle-to-plastic-transition (BPT) at varying temperatures. For many Al-containing phases and  $\text{Ti}_3\text{SiC}_2$ , this transition occurs between  $1,000^\circ\text{C}$  and  $1,100^\circ\text{C}$ . The drop in  $K_{Ic}$  above the BPT temperature rules out the activation of additional slip systems, leading to the categorization of this transition as a BPT rather than a ductile-to-brittle transition. The high-temperature response of MAX phases involves temperature-dependent grain boundary decohesion stress and/or delamination stress. Recent research confirms these conclusions, attributing the drop in  $K_{Ic}$  to a decrease in elastic modulus at higher temperatures. The response of  $\text{Ti}_3\text{SiC}_2$  to compressive cyclic loadings at high temperatures shows changes in stress-strain loops, with hardening observed at temperatures up to  $1,200^\circ\text{C}$ . Cycling results in microdomains that are harder to kink, affecting the stress-strain curves. Deformation at high temperatures reduces grain size by forming microdomains and/or kink bands. The response to tensile stresses is temperature and strain rate-dependent, with  $\text{Ti}_3\text{SiC}_2$  exhibiting plastic behavior above the BPT, with strains up to 25% without necking. The strain rate sensitivity of  $\text{Ti}_3\text{SiC}_2$  is high, resembling superplastic solids, but the deformation mechanisms differ due to grain size variations.[14]

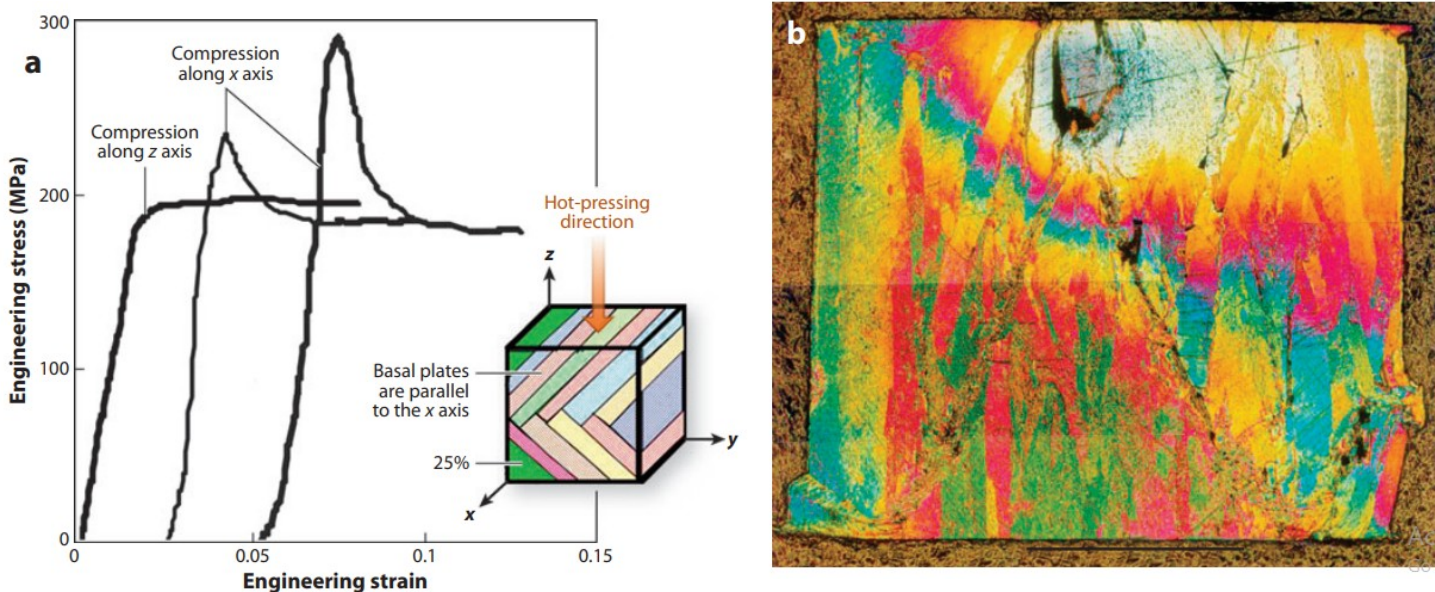


**Figure I.6.3.1 :** (a) Engineering stress-strain curves of 2-mm cubes of highly oriented samples of  $\text{Ti}_3\text{SiC}_2$ . The inset (right) shows a schematic of the cube and basal plane orientations. (b) Optical microscope micrograph of a polished and etched sample after deformation parallel to the basal planes. Note kinking at the corners. The kink band in the lower left corner generates a shear band that cuts across the cube face.[14]

### I.6.3.2 Room Temperature Mechanical Behavior :

The MAX phases exhibit anisotropic behavior in compression, with the response varying depending on the orientation of the basal planes. When the basal planes allow for slip, the samples yield at lower stress levels and deform by shear bands. In contrast, when the slip planes are parallel to the applied load, the stress-strain curves show maxima followed by strain softening and recovery. Deformation in this case occurs by a combination of kink band (KB) formation, delaminations within individual grains, and ultimately shear band formation. The KBs are potent suppressors of delaminations, contributing to the damage tolerance of the MAX phases. Not all MAX phases fail suddenly; some exhibit graceful failure characteristics with inverted shallow V-shaped stress-strain curves rather than sharp drops at maximum stress. This tendency increases with increasing grain size and reduced loading rates. The ultimate compressive, tensile, and flexural strengths of the MAX phases at room temperature are summarized in Table 3, with compressive strengths ranging from  $\approx 300$  MPa to close to 2 GPa, flexural strengths typically  $\approx 50\%$  lower than compressive strengths, and ultimate tensile strengths ranging from less than 100 MPa to  $\approx 300$  MPa. Larger-grained materials result in weaker solids.[14]

### I.6.4 Electronic properties :

The provided sources discuss the band structures and optical properties of non-superconducting materials, specifically focusing on MAX phases like  $Zr_2AC$  (where  $A = Al, Si, P,$  and  $S$ ). These materials exhibit a combination of metallic, covalent, and ionic bonding due to the differences in electronegativity between the elements involved. The DOSs at the Fermi level show a trend where there is a slight increase as the A-group element moves from left to right across the periodic table, followed by a decrease for S, leading to a transition to a more ceramic-like character in the S column. The interaction between A 3p states, Zr 4d states, C 2p, and C 2s states results in the formation of covalent Zr-A and Zr-C bonds, with strong Zr 4d-C 2p hybridization stabilizing the structures of  $Zr_2AC$ . These findings provide insights into the bonding nature and structural stability of MAX phases like  $Zr_2AC$ .

$Zr_2InC$		
	C-s	C-p
Bottom (eV)	-10,63	-9,04
Top (eV)	-5,08	-2,01

**Table 3 :** The theoretical calculations of the state's position of  $Zr_2InC$  (C-p and C-s)

### I.6.5 Thermal characteristics :

The Debye temperature ( $\theta_D$ ) is a critical factor in understanding the thermal behavior of MAX phases.  $\theta_D$  is related to various physical properties, including thermal expansion, thermal conductivity, melting temperature, specific heat, and lattice vibration. It also links the electron-phonon coupling factor and superconducting transition temperature in superconductors, and is related to the energy required to generate metal vacancies.

Anderson's technique, which uses the average elastic (sound) wave velocity, is a logical and straightforward method for calculating Debye temperature. **Table 4** presents the thermal characteristics of MAX phases, including the  $Zr_2AC$  MAX phase, where A can be Se, Si, P, Al, S, As, In, Ge, Sn, Tl, or Pb. The thermal properties, such as transverse, longitudinal, and average sound velocity ( $v_t$ ,  $v_l$ , and  $v_m$  in m/s), density ( $\rho$  in g/cm<sup>3</sup>), minimum thermal conductivity ( $K_{min}$  in W m<sup>-1</sup> K<sup>-1</sup>), and Debye temperatures ( $\theta_D$  in K), are analyzed for the  $Zr_2AC$  MAX phase. The density of MAX phases ranges from light (3.831 g/cm<sup>3</sup>) for  $Zr_2SnC$  to heavy (9.117 g/cm<sup>3</sup>) for  $Zr_2TiC$ , while Debye temperatures range from 679 K for  $Zr_2SeC$  to 350.0 K for  $Zr_2PbC$ . Other properties can be compared in a similar manner.[15]

p	Vl	Vt	Vm	OD	TCE ppm/K a (k-1)	Kmin
$Zr_2AlC$	5.29	5220	8093	5730	658.76	
$Zr_2InC$	7.1					
	7.1	4166	6640	4587	520.6	
					508.2	
					509.4	
$Zr_2TiC$	9.12	3870	6020	4249	481.52	
	9.36 8.92	5253	3145	3480	398	
		4989	2993	3311	372	
$Z_2SiC$	5.54	3777	6800	4207	490.32	
$Zr_2GeC$	6.54	3744	6461	4155	481.81	
	6.86	5998	3286	3664	432	
$Zr_2SnC$	7.28	3893	6465	4306	490.64	
	7.75	6111	3683	4073	472	
	3.83	6357	4236		482.75	
	3.89	6464	4305		490.64	
7.16					8.3 + 0.2	0

	7.16				
	6.9				
Zr <sub>2</sub> PbC	9.04	3524	5741	3890	438.45
	9.2				8.2 + 0.2 0.01
	9.1				
	8.2				
	9.04	2919	4920	3137	350
	8.87	2967	4984	3285	368.36
Zr <sub>2</sub> PC	6.03	4764	7842	5264	628.4
Zr <sub>2</sub> AsC	6.6	2669	5747	3006	348.56
Zr <sub>2</sub> SC	5.71	4826	7761	5319	622.73
	6.37	7494	4486	4964	603

**Table 4 :** Shows the determined transverse, longitudinal, average sound velocity ( $v_t, v_l$ , and  $v_m$  in m/s) and density ( $\rho$  in g/cm<sup>3</sup>), the minimum thermal conductivity  $K_{min}$  (W m<sup>-1</sup> K<sup>-1</sup>) and the debye temperatures ( $\theta_D$  in K) for the Zr<sub>2</sub>AC MAX phase.[15]

- so in conclusion, The crystal structure of MAX phases is a hexagonal framework with a space group of P6<sub>3</sub>/mmc, and there are various crystal structures such as 211, 312, 413, and 514, corresponding to  $n$  values of 1, 2, 3, and 4. The MAX phase compounds consist of a constant layer "A" and separate layers "M" and "X" affected by  $n$ , which influences their physical properties. The layered structure of MAX phases, where "X" layers are sandwiched between "M" layers and form MX blocks, is significant for their properties. The strong metallic bonds of M and X atoms and the weak bonds of M and A atoms, particularly in shear stress, contribute to the primarily metallic nature of MAX phases. The high elastic stiffness is due to the M-X bond, and the metallic bond of M-A provides electrical and thermal conductivity. These bonds give MAX phases their distinct metallic-ceramic characteristics, including thermal shock resistance, high-temperature plasticity deformation, easy machining, and strong thermal and electrical conductivity. They also have ceramic-like thermal expansion and high Young's modulus.

MAX phases have notable mechanical distinctions from their binary counterparts, MX carbides or nitrides, and offer more customization potential due to their three distinct intrinsic constituents. Adding atomic layers with different chemical compositions prevents dislocation motion and

strengthens the composite material. MAX phases are elastically rigid, with high melting points, outstanding strength at elevated temperatures, small expansion coefficients, and machinable, low-friction, and wear-resistant surfaces. They also resist corrosion, oxidation, fatigue, creep, and fracture, making them applicable in various fields. The combined properties of metal and ceramic on a macro scale, attributed to the structural and electronic characteristics of the layers of atoms that comprise the nanoscale constituents, make MAX phases a valuable material in various industries.

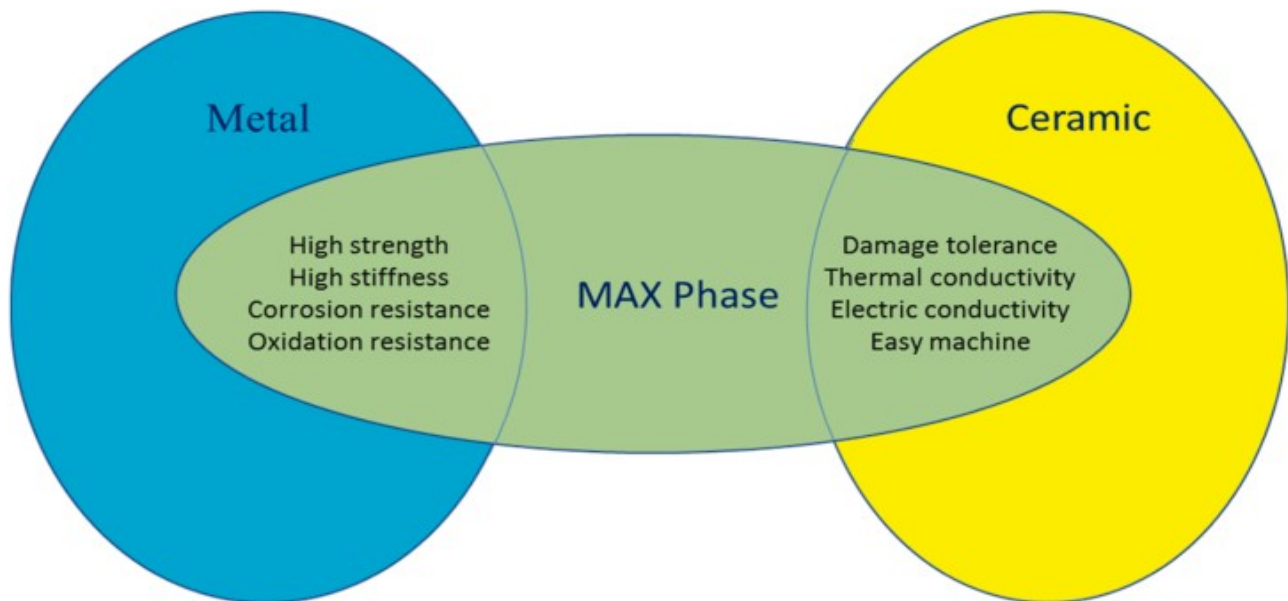


**Figure I.6 :** Characteristics of the MAX phase ceramics[15].

### I.7.State of the art:

**-Article 1:**Synthesis of Ti<sub>3</sub>SiC<sub>2</sub> MAX phase powder by a molten salt shielded synthesis (MS3) method in air (*May 2019 Journal of the European Ceramic Society 39(13)*)

The article "Lithography-based ceramic manufacturing (LCM) of 3Y-TZP with very high surface quality" published in the Journal of the European Ceramic Society in 2019 presents the state-of-the-art in lithography-based ceramic manufacturing (LCM) of 3 mol% yttria-stabilized tetragonal zirconia polycrystal (3Y-TZP) ceramics with a very high surface quality. The authors used 3Y-TZP with a relatively high surface area because it is a widely used universal ceramic material.

They investigated the LCM process, which involves two key quality-influencing steps: viscosity control and cleaning of the printed green parts.



The article demonstrates the ability of LCM to produce 3Y-TZP ceramics with a very high surface quality, which is crucial for applications such as dental restorations and cutting tools.

The authors used advanced characterization techniques like microtomography and image analysis to quantify the properties of the manufactured ceramics. Overall, this article represents the current state-of-the-art in lithography-based ceramic manufacturing of 3Y-TZP with a focus on achieving a very high surface quality, which is a critical requirement for many industrial applications of this material.[18]

**-Article 2:** Synthesis and Oxidation Testing of MAX Phase Composites in the Cr–Ti–Al–C Quaternary System by *(Denis Horlait, Salvatore Grasso, Nasrin Al Nasiri, Patrick A. Burr, William Edward Lee First published: 19 October 2015)*

The research article by Denis Horlait, Salvatore Grasso, Nasrin Al Nasiri, Patrick A. Burr, and William Edward Lee delves into the synthesis and oxidation testing of MAX phase composites within the Cr–Ti–Al–C quaternary system. This study contributes significantly to the field of materials science and engineering by exploring the properties and behavior of MAX phase materials in a specific compositional range.

The theoretical foundation of MAX phases, known for their unique combination of metallic and ceramic properties, forms the basis of this research. The study's focus on the Cr–Ti–Al–C quaternary system is particularly relevant due to the potential for tailored properties and enhanced performance in high-temperature applications.

The article details the synthesis methods employed to fabricate MAX phase composites in the specified quaternary system. The innovative approaches and techniques utilized in the synthesis process demonstrate a commitment to advancing the understanding and production of these materials.

Through rigorous oxidation testing, the authors have provided valuable insights into the oxidation behavior and performance of the MAX phase composites. The results offer a comprehensive analysis of the materials' response to high-temperature environments, shedding light on their stability and potential applications in extreme conditions.

This research significantly advances the knowledge of MAX phase composites in the Cr–Ti–Al–C system, highlighting their potential for use in aerospace, energy, and other demanding industries. The findings presented in this study pave the way for further exploration of these materials, including optimization of properties, scalability of synthesis methods, and practical applications in real-world scenarios.

In conclusion, the work by Horlait et al. represents a significant contribution to the field of materials science, offering a comprehensive analysis of MAX phase composites in the Cr–Ti–Al–C quaternary system. This state of the art underscores the importance of continued research in this area to unlock the full potential of these advanced materials.[17]

### **I.8.Conclusion :**

In conclusion, Ordered MAX phases represent a unique class of materials with a rich history and a wide range of properties that make them suitable for various applications. The crystal structure of MAX phases is characterized by the presence of a hexagonal lattice, which gives them a unique combination of metallic and ceramic properties. The electronic structure of MAX phases is also complex, with a mix of metallic and covalent bonding that contributes to their unique properties. The microstructure of MAX phases plays a crucial role in determining their properties, and various elaboration techniques can be used to control the microstructure, including combustion synthesis, hot pressing, spark plasma sintering, and molten salt synthesis. These techniques allow for the production of MAX phases with tailored microstructures and properties. MAX phases exhibit a range of properties, including elastic properties, nonlinear elastic behavior, mechanical properties, electronic properties, and thermal characteristics. These properties make MAX phases suitable for various applications, including high-temperature mechanical behavior, room temperature mechanical behavior, electronic devices, and thermal management. Overall, MAX phases represent a fascinating and important class of materials, and further research is needed to fully understand and optimize their properties for various applications.



# Chapter II:

## Experimentation techniques

## **Introduction:**

The primary objective of this research is to investigate the synthesis of  $\text{Cr}_2\text{Ti AlC}_2$  MAX phase materials through a combination of cold uniaxial compaction and subsequent heat treatment.

Furthermore, this study aims to identify the phases present in the developed materials using various experimental characterization techniques.

In pursuit of the aforementioned goals, the researchers have explored a novel experimental approach known as the molten salt method. This method involves the use of specific salts, namely KBr, which has been previously reported in the literature. However, to the best of the authors' knowledge, the present study represents the first instance of employing KCl salt in this context.

## **Methodology:**

The synthesis of MAX phase materials was carried out using a two-step process. First, cold uniaxial compaction was employed to shape the raw materials into the desired form. Subsequently, the compacted samples underwent heat treatment to facilitate the formation of the target  $\text{Cr}_2\text{Ti AlC}_2$  MAX phase.

To identify the phases present in the developed materials, a range of experimental characterization techniques were utilized. These techniques were carefully selected to provide comprehensive insights into the composition, structure, and properties of the synthesized materials.

### **II.1.1 The $\text{Cr}_2\text{Ti AlC}_2$ MAX phase synthesis:**

The molten salt technique is widely used for sintering MAX phases, the primary powder mix consists of the elements (Ti, Cr, Al and C).

The preparation of the samples will be powders according to their final form, the technique used will be done in a High-Temperature Tube Furnaces for Horizontal or Vertical Operation up to 1800 °C in an under-air atmosphere, to inhibit the oxidation of the powders, we will:

- synthesise the MAX phase  $\text{Cr}_2\text{Ti AlC}_2$  and  $\text{Cr}_2\text{Ti Al}_{1,2}\text{C}_2$  using KCl in different temperatures at the LERTI laboratory University of Blida 1 and the Research Center in Industrial Technologies CRTIDZ.

#### 1.1 Powders used:

below are the powder mix used to synthesize the  $\text{Cr}_2\text{Ti AlC}_2$  MAX phase:

Titanium carbide (Ti), Aluminum (Al) and Chromium (Cr), Carbon (graphite) (C).

Elements	Powder size	Brand	Purity	Molar mass
Ti				
Cr	400 mesh	BIOCHEM	0.99	52
Al	25 microns	PROLABO	0.99	26.98
C	2 microns	PROLABO	1	12.01

Table 5: tribological conditions used for the composite systems.

The figure below shows the powder reagents used in the study:

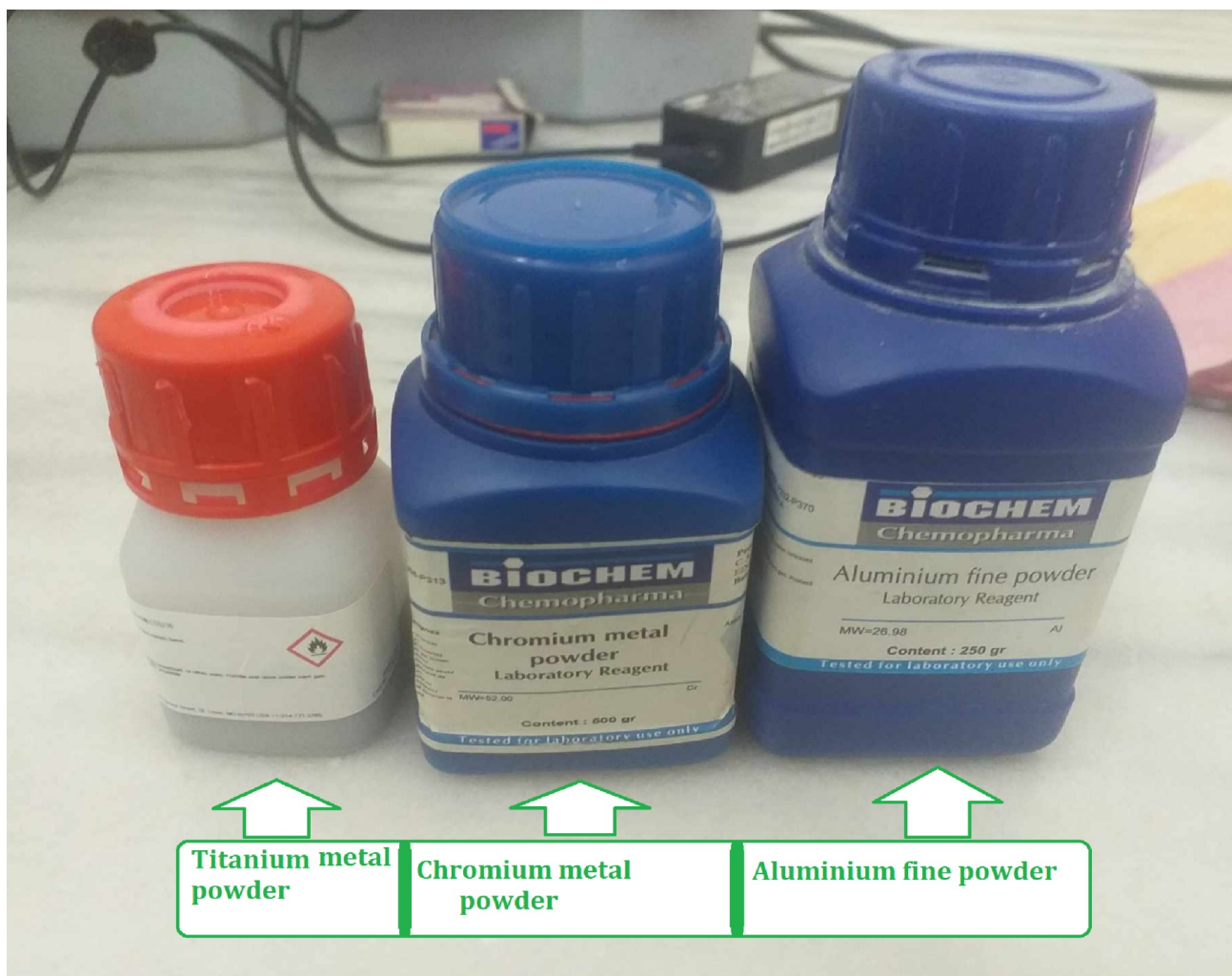


Figure II. 1: powder reagents used in our experiment

### II.1.2 Weighing the powder:

First of all we made a homogeneous mixture of powders for 2 samples each sample 5g (gram)

- First sample: the phase  $\text{Cr}_2\text{TiAlC}_2$  ( $n_{\text{Cr}} = 2 \text{ mol}$  ;  $n_{\text{Ti}} = 1 \text{ mol}$  ;  $n_{\text{Al}} = 1 \text{ mol}$  ;  $n_{\text{C}} = 2 \text{ mol}$  )
- Second sample: the phase  $\text{Cr}_2\text{TiAl}_{1.2}\text{C}_2$  ( $n_{\text{Cr}} = 2 \text{ mol}$  ;  $n_{\text{Ti}} = 1 \text{ mol}$  ;  $n_{\text{Al}} = 1.2 \text{ mol}$  ;  $n_{\text{C}} = 2 \text{ mol}$  )

The mix in gram	Cr mass in g	Ti mass in g	Al mass in g	C mass in g
$\text{Cr}_2\text{TiAlC}_2$	2.5	1.15	0.78	0.58
$\text{Cr}_2\text{TiAl}_{1.2}\text{C}_2$	2.56	1.18	0.6637	0.59

**Table 6 :** Elaborated samples mass in gram.

the method used to calculate the mass of each element:

$$\text{We have: } \left\{ \begin{array}{l} n_t = \frac{m_t}{M_t} \\ M_t = \sum_i^n n_i M_e / \quad M_e = M \times n \end{array} \right.$$

$$m_a = n_t \times M_e$$

with:

**n<sub>t</sub>**: the amount of total matter (molecule). in (mol)

**n<sub>a</sub>**: the mass of an atom (element) In (g)

**M<sub>t</sub>**: the total molar mass (sample) in (U)

**M<sub>e</sub>**: the molar mass of an element. in (U)

**M**: the molar mass. in (U)

**n**: stoichiometric number.

**Examples:**

first sample: **Cr<sub>2</sub>TiAlC<sub>2</sub>**

$$\mathbf{n}_{Cr_2TiAlC_2} = \frac{m_{Cr_2TiAlC_2}}{M_{Cr_2TiAlC_2}}$$

$$\mathbf{M}_{Cr_2TiAlC_2} = \sum_i^n \square \mathbf{M}_e = 2 \times \mathbf{M}_{Cr} + \mathbf{M}_{Ti} + \mathbf{M}_{Al} + 2 \times \mathbf{M}_C$$

$$\mathbf{M}_{Cr_2TiAlC_2} = (2 \times 51.9961) + 47.867 + 24.981539 + (2 \times 12.01)$$

$$\mathbf{M}_{Cr_2TiAlC_2} = 202.867 \text{ mol/m}$$


$$\mathbf{n}_{Cr_2TiAlC_2} = \frac{5}{202.867} = 0.0246$$

**Therefore**

- **m<sub>Cr</sub>** = 51.9961 × 2 × 0.0246 = 2.5582g
- **m<sub>TiC</sub>** = 47.867 × 0.0246 = 1.1775g
- **m<sub>Al</sub>** = 26.981539 × 0.0246 = 0.6637g
- **m<sub>C</sub>** = 12.01 × 2 × 0.0246 = 0.5908 g

**Note:** the same method applies to the second sample.

The powders were weighed using a 0.0001g precision balance (Figure II.3) at the LERTI Industrial Technology Study and Research Laboratory (University of Blida1).

We add a quantity of 8g once with the Kcl. We obtain at the end:

- Two mixtures of  $\text{Cr}_2\text{TiAlC}_2$  and  $\text{Cr}_2\text{TiAl}_{1.2}\text{C}_2$  with Kcl.

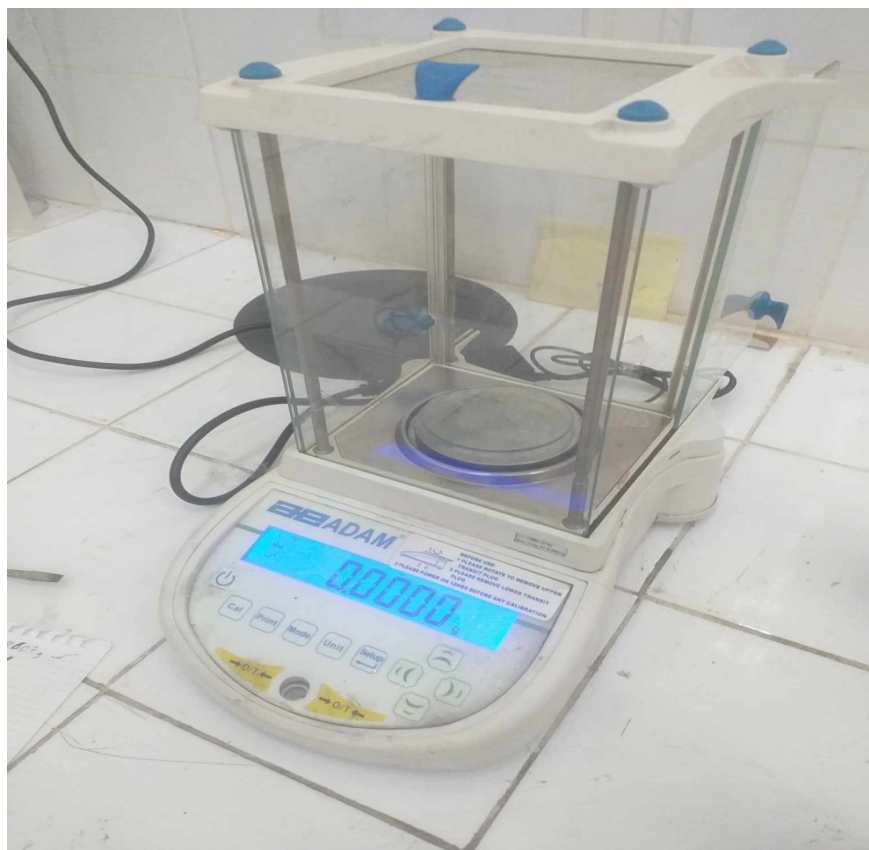


**Figure II.3:** precision analytical balance ADAM

### **II.1.3 Grinding :**

Each blend was milled using an agate mortar, and the resulting powders were transferred to containers. To ensure homogeneity, balls were added and the powders were agitated for a period of 72 hours to achieve uniform mixing.



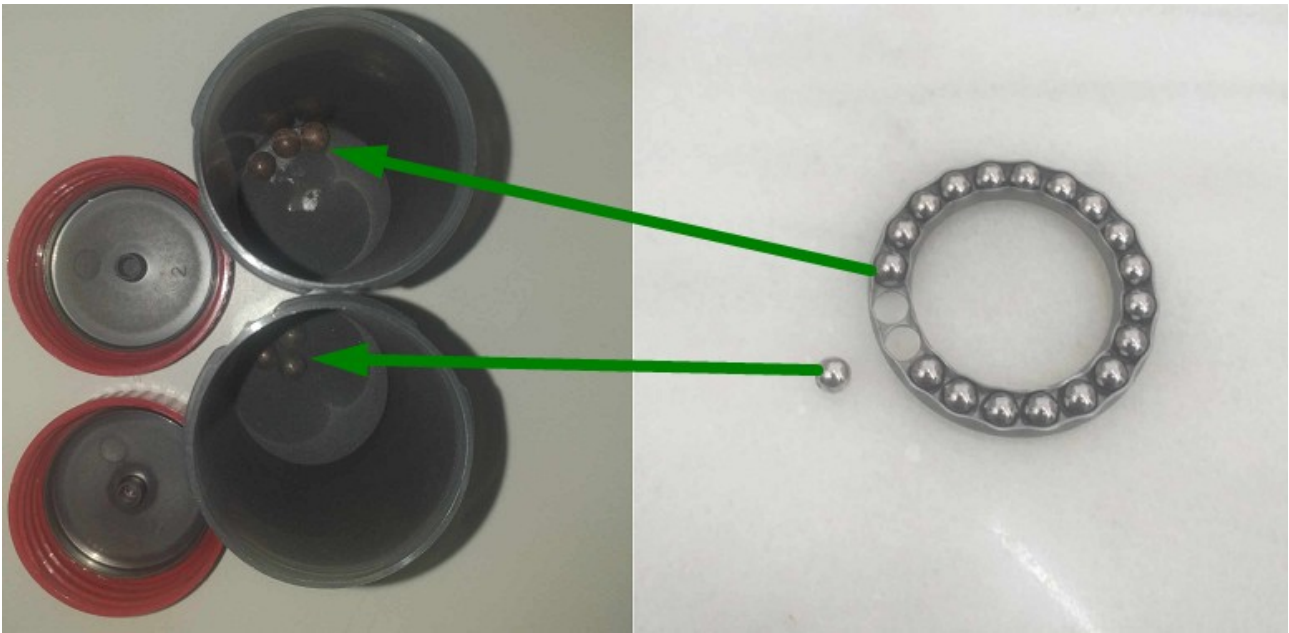


Figure II.4: homogenized powder through baring balls.

#### **II.1.4 cold compaction :**

after weighting the powder mix, grinding, and mixing, it comes to the compaction stage, using the compaction tool shown in **Figure II.5** the powder inside this last is then put in a manual hydraulic pellet press - Specac Ltd shown in **Figure II.6** to become a pill (tablet) as we can see in **Figure II.7**, the pressure applied is 5 bar.



**Figure II.5 :** powder compaction tool.



**Figure II.6 :** Manual Press 25 ton Hydraulic Pellet Press - Specac Ltd

This process was made in L.E.R.T.I laboratory University Saad Dahlab Blida 01.

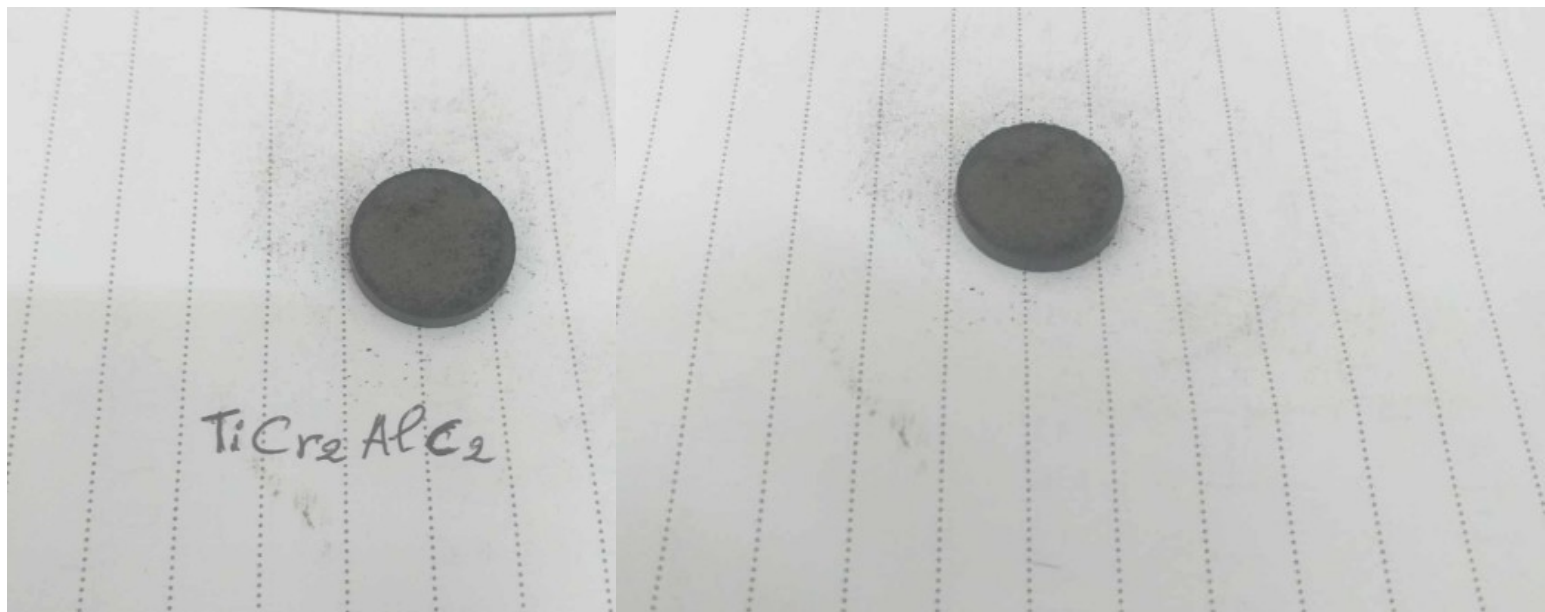


**Figure II.7 :** sample tablet after compaction in the manual press

## II.1.5 Sel encapsulation :

we put out previously pressed sample tablet in another device shown in the **Figure II.8** along with our protective salt (potassium chloride) in our case to be encapsulated within this last using the same Manual Press shown previously in **Figure II.6** , for this will form a thic layer that protect our sample from oxidation in heat treatment process at the same pressure (5bar).

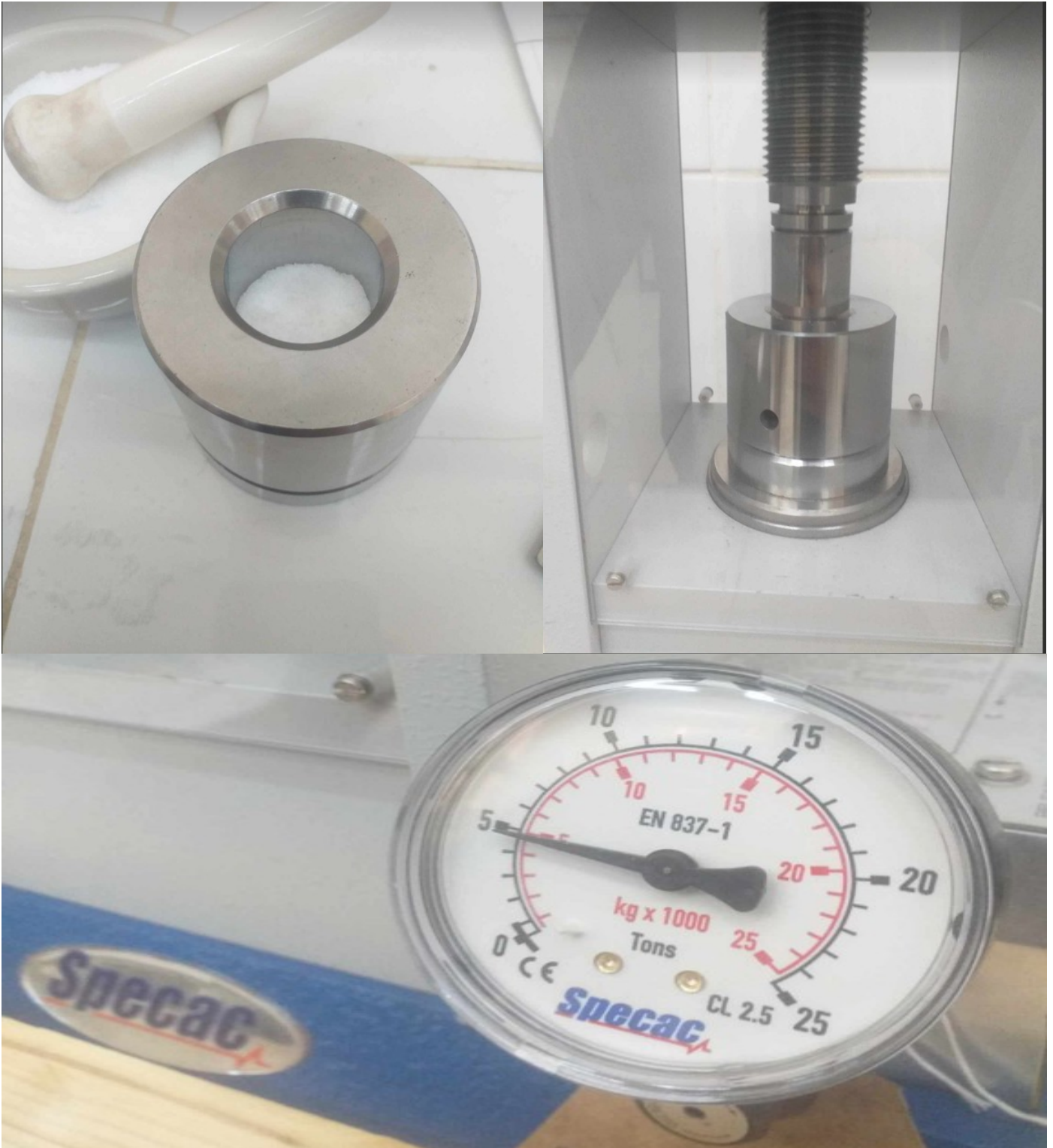


**Figure II.8 :** encapsulation/compaction tool and the pressure applied.

After compaction the samples will be a solid capsule as we can see in **Figure II.9**

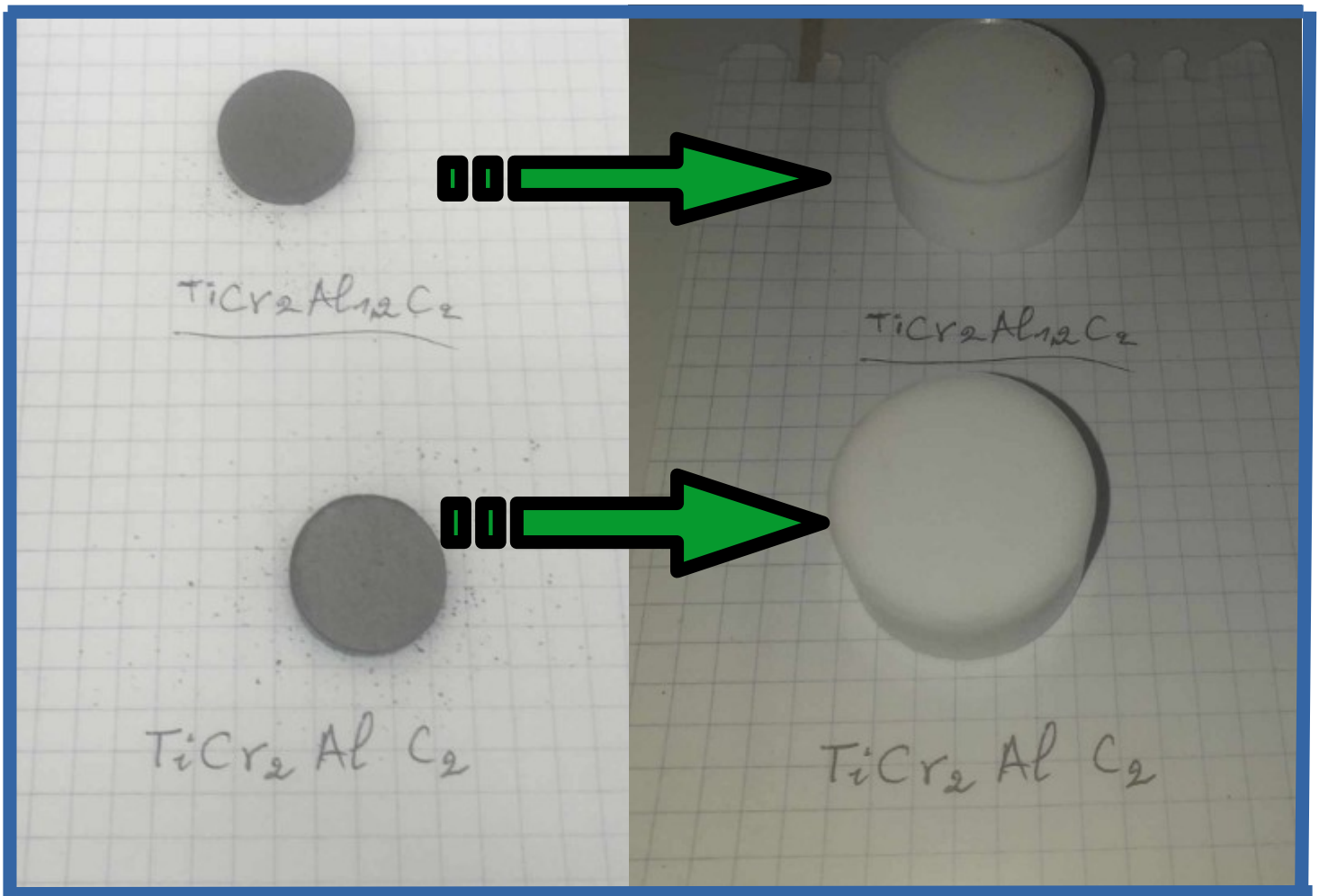


**Figure II.9 :** samples before and after encapsulation

## **II.1.6 Heat treatment by sintering:**

### **II.1.6.1 sample pot preparation:**

before exposing our samples to heat treatment, we first immerse this last in sintering pot made of porcelain. First we fill 25% of the pot with potassium chloride (powder), we put our sample on top, then we fill the rest with more potassium chloride powder. this way our encapsulated sample's salt will be the last thing to melt, therefore this last should be protected from oxidation during our sintering process.



The following figure shows the pot filling steps, as we can notice how the sample is being submerged inside the salt powder.

**Figure II.10:** sintering pot filling steps.

Next we put the pot in the furnace and set the heat temperature per minute at  $5^{\circ}\text{C}/\text{min}$ :

- ▣ For  $1000^{\circ}\text{C}$  it took 3h:20 min to reach high temperature with 2h of holding.
- ▣ For  $1050^{\circ}\text{C}$  it took 3h:30 min to reach high temperature with 2h of holding.
- ▣ For  $1200^{\circ}\text{C}$  it took 4h:00 min to reach high temperature with 2h of holding.

In all the previous cases, the sample is left to cool down inside the furnace.

### II.1.6.2 the furnace process:

in this process we used the muffle furnace Nabertherm B180 present at L.E.R.T.I laboratory at Saad Dahleb University for temperatures below 1100°C, and for higher temperatures we used the tubular furnace (Nabertherm GmbH) present at C.R.T.I cheraga research center.



**Figure II.11:** Tubular furnace Nabertherm GmbH 1800°C

the following figure shows the sample inside the Tubular furnace Nabertherm GmbH 1800°C



**Figure II.12:** sample inside the Tubular furnace Nabertherm GmbH 1800°C at C.R.T.I cheraga research Center.



**Figure II.13:** furnace Nabertherm B180

### **II.1.7 powders recovery:**

as soon as the furnace timer is done and the sample is reasonably cooled down, the sample is then taken to L.E.R.T.I laboratory at Saad Dahleb University to recover our compressed sample from the cold solid state salt.

The following figure show the sample pot after being recovered from our furnace



**Figure II.14:** sample pot state after recovery from the furnace.



Using water and a stainless steel spatula, we gradually melt the solidified slat to liberate the sample inside. Once we have this last freed, we put it in a becher with water, we also slip in a magnetic rod, and put this becher upon a magnetic stirrer/heater shown in the following figure.

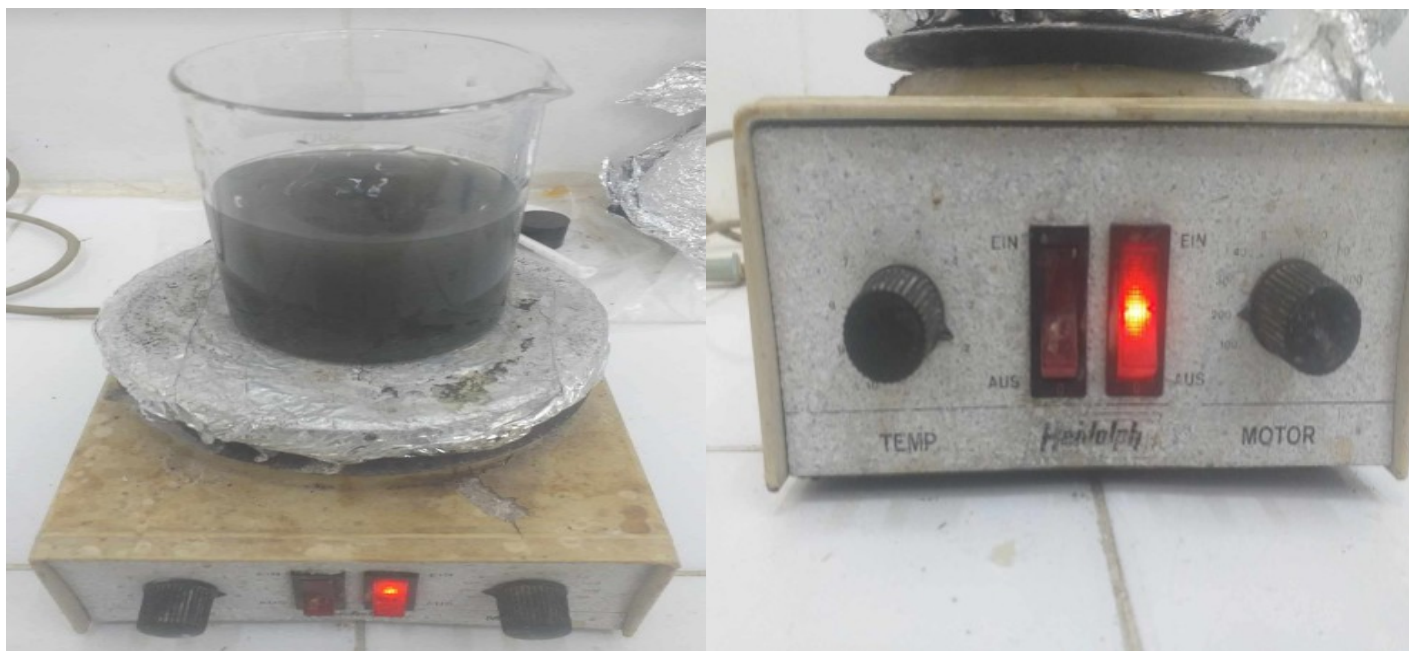


**Figure II.15:** magnetic stirrer/heater Heifolph.

Once the dissolution is done and the sample is back to powder state inside the becher we stop the magnetic stirrer/heater and prepare a filter, a funnel, and a Conical flask/Erlenmeyer flask as shown in the next figure, and pour the liquid upon the filter, and keep rinsing the powder from residual salt with water.



**Figure II.16:** the filtering/rinsing process tools (Conical flask/Erlenmeyer, filter, plastic funnel)  
- The next step is to put the filter in a Petri dish to be left in the laboratory oven until dry. The following figure shows the oven used to dry the powder.



**Figure II.17:** Memmert Single Display UN Series Universal Oven.

## **II.2. Microstructural Characterization:**

after all the previous steps, our powder is now ready to be inspected to find out what new phases are present in this last. To do that, the proper operation is XRD (X Ray Diffraction).

### **II.2.1 X Ray Diffraction and Bragg's law:**

X-ray diffraction (XRD) is a non-destructive analytical technique that exploits the wave nature of X-rays to probe the crystallographic structure of materials. Its effectiveness lies in the wavelength of X-rays, which is on the order of the interatomic distances within crystals. This allows for constructive and destructive interference of scattered X-rays, providing valuable information about the underlying atomic arrangement.

## **Theoretical Framework:**

**II.2.1.1. Interaction with Electron Clouds:** X-rays interact primarily with the electron cloud surrounding each atom in the sample. The scattering intensity is proportional to the electron density distribution within the material.

**II.2.1.2. Constructive and Destructive Interference:** When a collimated beam of X-rays impinges on a crystalline sample, the incident radiation interacts with the electron cloud of each atom. These interactions lead to the scattering of X-rays in various directions. However, in a crystalline material, the ordered arrangement of atoms acts as a diffraction grating for the scattered waves.

- **Constructive Interference:** If the scattered X-rays from different atomic planes travel in phase (crest meets crest) due to the specific atomic spacing and the incident angle, they undergo constructive interference, resulting in a strong diffracted beam at a particular angle ( $\theta$ ). This phenomenon is governed by Bragg's Law:

$$n\lambda = 2d \sin(\theta)$$

where  $n$  is an integer (order of reflection),  $\lambda$  is the X-ray wavelength,  $d$  is the interplanar spacing in the crystal, and  $\theta$  is the diffraction angle.

- **Destructive Interference:** Conversely, if the scattered waves are out of phase due to the atomic arrangement, they undergo destructive interference, leading to a weak or absent signal at that particular angle.

**II.2.1.3 Experimental Observations:** The diffracted X-ray beam is detected using a movable detector, recording the intensity as a function of the diffraction angle ( $2\theta$ ). This recorded pattern, known as the diffractogram, is a characteristic fingerprint of the crystal structure. Each set of diffracting planes within the crystal lattice contributes to a peak in the diffractogram at a specific angle determined by Bragg's Law.

**II.2.1.4 Structural Analysis:** By analyzing the positions and intensities of the peaks in the diffractogram, scientists can extract valuable crystallographic information:

- **Crystal Structure Determination:** The positions of the peaks provide information about the unit cell dimensions and the arrangement of atoms within the unit cell. This allows for the determination of the crystal system (geometry of the unit cell) and the space group (symmetry elements).
- **Phase Identification:** By comparing the diffractogram with known reference patterns in databases, scientists can identify the unknown material in a sample.

- Crystallite Size and Strain Analysis: The broadening of diffraction peaks can be correlated with the average crystallite size and the presence of strain within the crystal lattice

In our work, diffractograms are recorded upon the radiation ( $\text{CuK}\alpha$   $\lambda= 1.5406 \text{ \AA}$ ) on a powder specialized diffractometer of the type Bruker D2 PHASER 2G present in C.R.T.I research center in Cheraga shown in **figure II.18**, within the angular domain of  $5^\circ$ - $90^\circ$  on a step of  $0,05^\circ$  counting 1second between each step.



**Figure II.18** Diffractometer Bruker D2 PHASER.

# **Chapter III**

**Results presentation**

**&**

**Interpretation**

### **III.1 Introduction:**

this chapter will include our experimental results, our experiment consist of synthesizing the Ordered MAX phase of  $\text{Cr}_2\text{TiAlC}_2$  through molten salt method, in our case we used **KCl**, this experiment was processed under different temperatures (1000°C, 1100°C and 1300°C), then we analyzed our product powder by XRD.

We used molten salt as a protective agent in our synthesis process to achieve our objective. This allowed us to avoid the need for an argon gas furnace and lower the temperature required for the synthesis of MAX phase materials. Specifically, we chose to use potassium chloride (KCl) for this purpose.

The synthesis of ceramic powders with controlled composition, morphology, and crystalline phase can be effectively achieved using molten salt techniques. This approach offers the advantage of operating at relatively low temperatures, without the need for an argon gas furnace.

### III.2. X ray diffraction analysis of the powders $\text{Cr}_2\text{TiAlC}_2$ & $\text{Cr}_2\text{TiAl}_{1.2}\text{C}_2$ with Potassium Chloride KCl at $1000^\circ\text{C}$ - $1100^\circ\text{C}$ - $1300^\circ\text{C}$ .

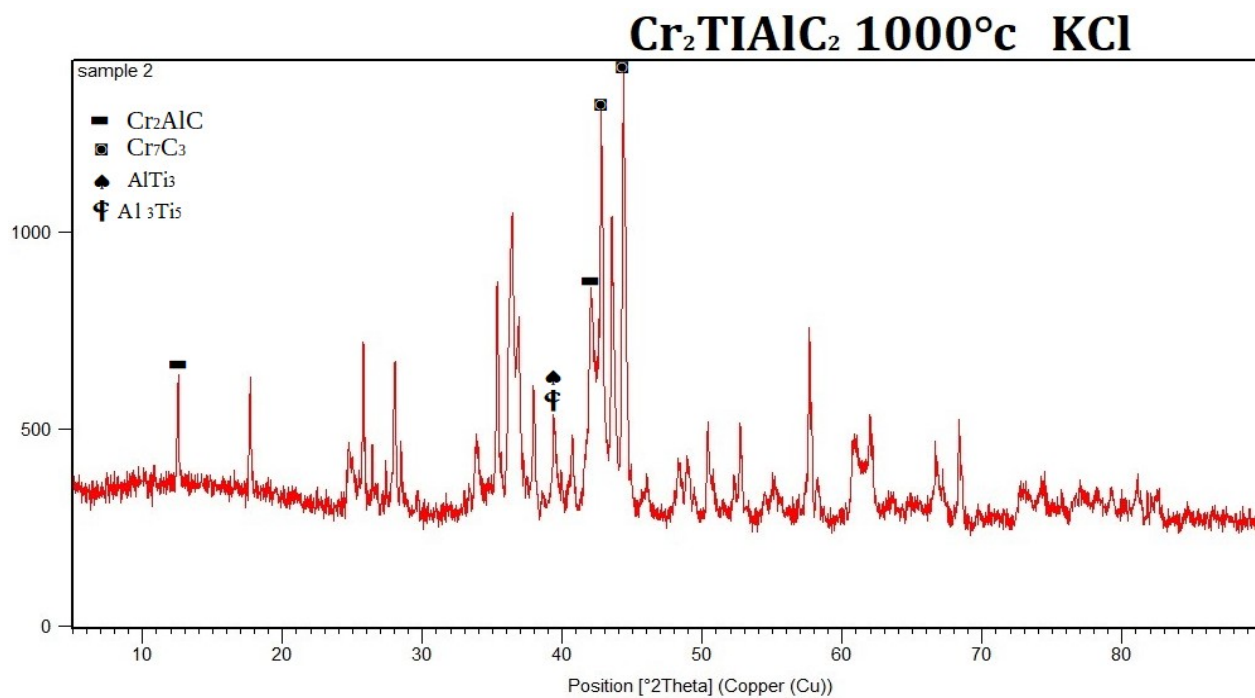


Figure III.1: XRD graph for the sample  $\text{Cr}_2\text{TiAlC}_2$  at  $1000^\circ\text{C}$  coated with potassium chloride.

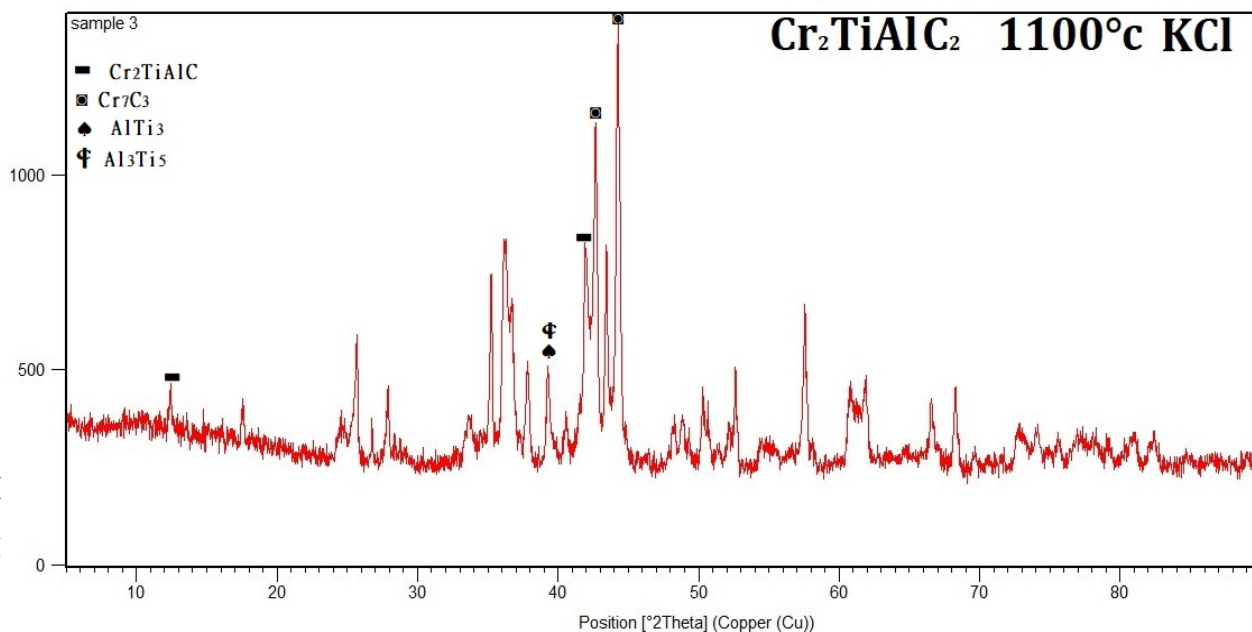
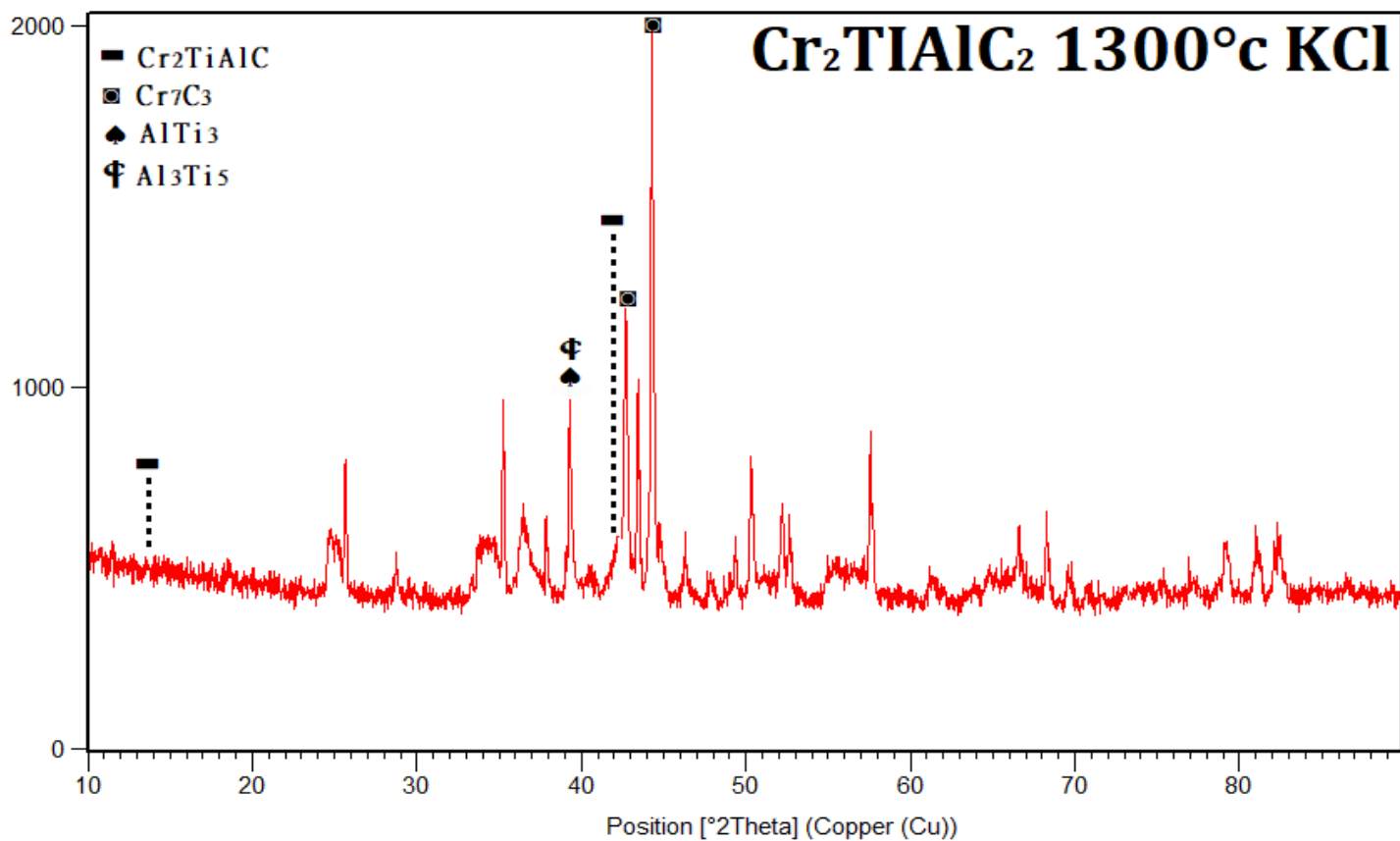


Figure III.2: XRD graph for the sample  $\text{Cr}_2\text{TiAlC}_2$  at  $1100^\circ\text{C}$  coated with potassium chloride.





**Figure III.3:** XRD graph for the sample Cr<sub>2</sub>TiAlC<sub>2</sub> at 1300°C coated with potassium chloride.

### III.3 Comparison of the three X Ray Diffraction graphs:

to have a convenient perspective on the previous XRD graphs, we are stacking these for better comparison:

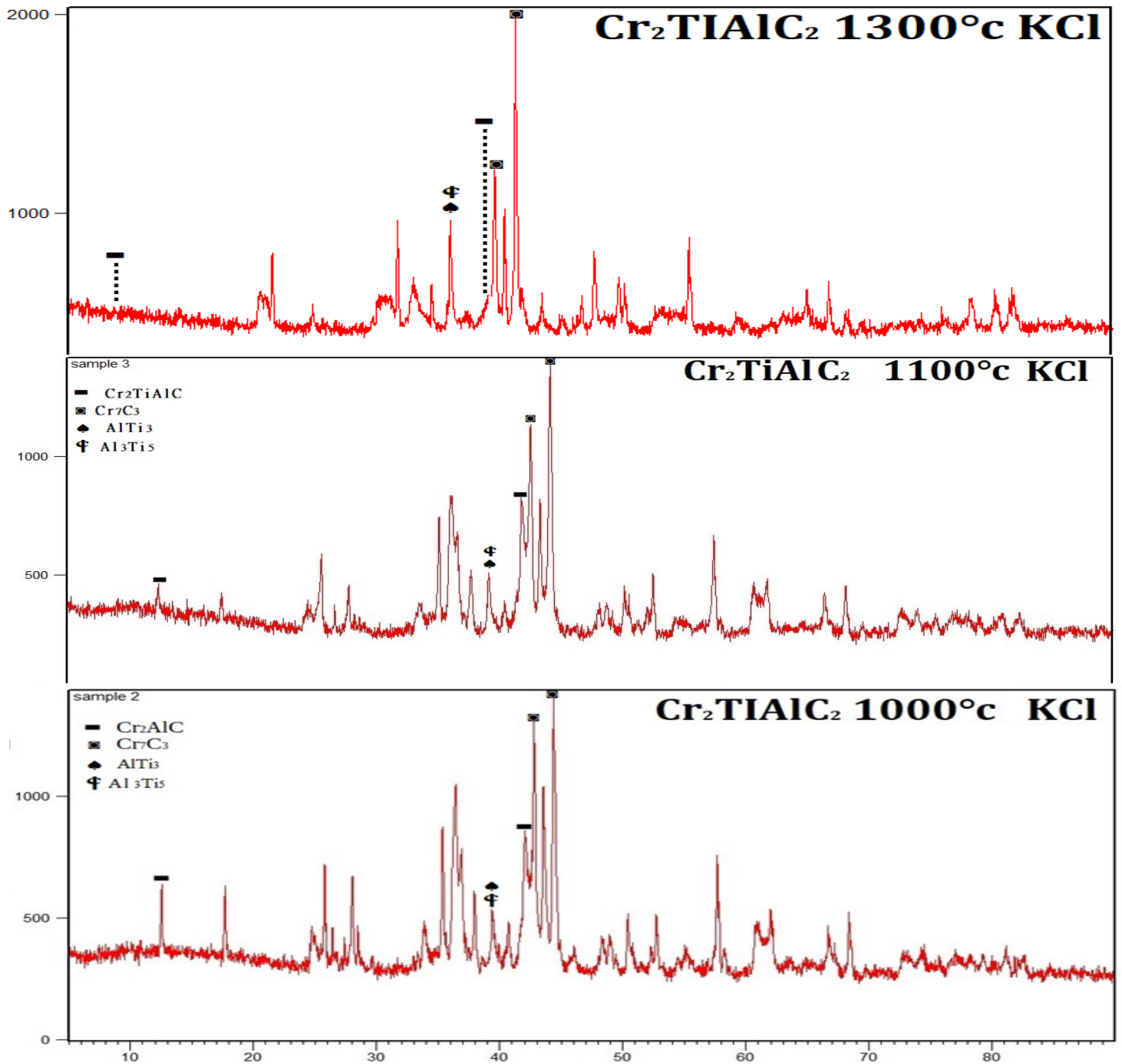


Figure III.4: XRD for the three samples stacked for comparison.

Observations and discussion :

- ▶ In the lowest temperature 1000°C, we were able to identify the phases (Cr<sub>2</sub>TiAlC; Cr<sub>7</sub>C<sub>3</sub>; AlTi<sub>3</sub>; Al<sub>3</sub>Ti<sub>5</sub>)
- ▶ As temperature reached 1100°C, we can notice that the phase Cr<sub>2</sub>TiAlC is slowly fading while the phases AlTi<sub>3</sub> and Al<sub>3</sub>Ti<sub>5</sub> are growing in terms of magnitude.
- ▶ As for the high temperature of 1300°C, we can see that the phase Cr<sub>2</sub>TiAlC is no more, as the other two phases continues rising.
- ▶ Unfortunately, we do not see the phase that we aimed for which is Cr<sub>2</sub>TiAlC<sub>2</sub>.

### III.4. Final analysis and conclusion:

Usually, MAX phases are synthesized in a higher temperature (around 1450-1500°), to lower the required temperature for our samples reagents to react with each other, we used salts like KCl, which is one major contributor in our hypothesis.

At first we thought that we didn't reach the required temperature for this phase formation, but as we received the previously shown data very recently, we realized that the exact opposite hypothesis is way more logical.

now, our new hypothesis dictates that we did reach that phase in temperatures even lower than 1000°C, and as temperature rise our phase began to decompose as follows:



And as temperature kept rising as well as the salt influence on reactivity, the phase Cr<sub>2</sub>TiAlC decomposed by its turn into chromium carbides and titanium based intermetallic

## **Referances: in the APA citation 7<sup>th</sup> edition.**

- [1] González-Julián, J. (2020). Processing of MAX phases: From synthesis to applications. *Journal of the American Ceramic Society*, 104(2), 659–690. <https://doi.org/10.1111/jace.17544>
- [2] Barsoum, M. W. & El-Raghy, T. Synthesis and characterization of a remarkable ceramic: Ti<sub>3</sub>SiC<sub>2</sub>. *J. Am. Ceram. Soc.* 79, 1953–1956 (1996).
- [3] Eklund, P., Beckers, M., Jansson, U., Högberg, H., & Hultman, L. (2010). The M+1AX phases: Materials science and thin-film processing. *Thin Solid Films*, 518(8), 1851–1878. <https://doi.org/10.1016/j.tsf.2009.07.184>
- [4] Chemical bonding and electronic-structure in MAX phases as viewed by Xray spectroscopy and density functional theory. (n.d.). *Thin Solid Films*, 621. <https://www.diva-portal.org/smash/get/diva2:1052391/FULLTEXT03>
- [5] Li, Y., Wei, H., Chen, L., Xie, C., Ding, H., Fang, F., Chai, Z., & Huang, Q. (2024). Regulating the electronic structure of MAX phases based on rare Earth element SC to enhance electromagnetic wave absorption. *ACS Nano*. <https://doi.org/10.1021/acsnano.3c11585>
- [6] Low, I., & Zhou, Y. (n.d.). *MAX Phases: Microstructure, Properties, and Applications*.
- [7] Nieświec, M., & Sadowski, Ł. (2021). The assessment of strength of cementitious materials impregnated using hydrophobic agents based on Near-Surface Hardness measurements. *Materials (Basel)*, 14(16), 4583. <https://doi.org/10.3390/ma14164583>
- [8] Истомина, П. В., Истомина, Е. И., Надуткин, А. В., Ваева, О., Морokhina, А., & Грасс, В. Э. (2024). Key reaction steps in the combustion synthesis of Ti<sub>3</sub>SiC<sub>2</sub>/SiC ceramic composites using titanium reactant in foil form: Microstructural evidence. *Open Ceramics*, 18, 100585. <https://doi.org/10.1016/j.oceram.2024.100585>
- [9] Li, C., Zhang, X., Wang, K., Sun, X., & Ma, Y. (2021). Magnesiothermic sequestration of CO<sub>2</sub> into carbon nanomaterials for electrochemical energy storage: A mini review. *Electrochemistry Communications (Print)*, 130, 107109. <https://doi.org/10.1016/j.elecom.2021.107109>
- [10] Khalil, Abdelrazek. (2012). Advanced Sintering of Nano-Ceramic Materials. 10.5772/38287.
- [11] Guillon, O., González-Julián, J., Dargatz, B., Kessel, T., Schierner, G., Räthel, J., & Herrmann, M. (2014). Field-Assisted Sintering Technology/Spark Plasma Sintering: Mechanisms, materials, and technology developments. *Advanced Engineering Materials*, 16(7), 830–849. <https://doi.org/10.1002/adem.201300409>
- [12] Chen, J., Jin, Q., Li, Y., Shao, H., Liu, P., Liu, Y., Taberna, P., Huang, Q., Lin, Z., & Simon, P. (2022). Molten Salt-Shielded synthesis (MS3) of MXenes in air. *Energy & Environment Materials*, 6(2). <https://doi.org/10.1002/eem2.12328>

- [13] Amrillah T, Abdullah CAC, Hermawan A, Sari FNI, Alvani VN. Towards Greener and More Sustainable Synthesis of MXenes: A Review. *Nanomaterials (Basel)*. 2022 Dec 1;12(23):4280. doi: 10.3390/nano12234280. PMID: 36500902; PMCID: PMC9793760.
- [14] Barsoum, M. W., & Radović, M. (2011). Elastic and mechanical properties of the MAX phases. *Annual Review of Materials Research (Print)*, 41(1), 195–227.  
<https://doi.org/10.1146/annurev-matsci-062910-100448>
- [15] Hussein, D. R., Abbas, K. K., & Al-Ghaban, A. (2023). Overview of structural, electronic, elastic, thermal, optical, and nuclear properties of Zr<sub>2</sub>AC (A= Al, Si, P, S, Ge, As, Se In, Sn, Tl, and Pb) MAX phases: A brief review. *Heliyon*, 9(8), e18303.  
<https://doi.org/10.1016/j.heliyon.2023.e18303>
- [16] A.Souchet « Comportement tribologique d'une phase MAX : Transition et effets d'échelle sur différents Ti<sub>3</sub>SiC<sub>2</sub> »,2004
- [17] Horlait, D., Grasso, S., Nasiri, N. A., Burr, P. A., & Lee, W. E. (n.d.). Synthesis and Oxidation Testing of MAX Phase Composites in the Cr–Ti–Al–C Quaternary System. *Journal of the American Ceramic Society*. <https://doi.org/10.1111/jace.13962>
- [18] Dash, A., Sohn, Y. J., Vaßen, R., Guillon, O., & Gonzalez-Julian, J. (2019). Synthesis of Ti<sub>3</sub>SiC<sub>2</sub> MAX phase powder by a molten salt shielded synthesis (MS3) method in air. *Journal of the European Ceramic Society*, 39(13), 3651–3659.  
<https://doi.org/10.1016/j.jeurceramsoc.2019.05.011>